

Nodule-specific Cu⁺-chaperone NCC1 is required for symbiotic nitrogen fixation in *Medicago truncatula* root nodules

Cristina Navarro-Gómez¹ , Javier León-Mediavilla¹, Hendrik Küpper^{2,3} , Mario Rodríguez-Simón¹, Alba Paganelli-López^{1,4} , Jiangqi Wen⁵, Stefan Burén^{1,4} , Kirankumar S. Mysore⁵ , Syed Nadeem Hussain Bokhari² , Juan Imperial¹ , Viviana Escudero¹  and Manuel González-Guerrero^{1,4} 

¹Centro de Biotecnología y Genómica de Plantas, Universidad Politécnica de Madrid (UPM)-Instituto Nacional de Investigación y Tecnología Agraria y Alimentaria (INIA/CSIC), Campus de Montegancedo UPM, Pozuelo de Alarcón, Madrid, 28223, Spain; ²Laboratory of Plant Biophysics and Biochemistry, Institute of Plant Molecular Biology, Biology Centre, Czech Academy of Sciences, Ceske Budejovice, 37005, Czech Republic; ³Department of Experimental Plant Biology, Faculty of Sciences, University of South Bohemia, Ceske Budejovice, 37005, Czech Republic; ⁴Department of Biotechnology-Plant Biology, Escuela Técnica Superior de Ingeniería Agraria, Alimentaria y de Biosistemas, Universidad Politécnica de Madrid, Madrid, 28040, Spain; ⁵Institute for Agricultural Biosciences, Oklahoma State University, Ardmore, OK 73401, USA

Summary

Authors for correspondence:
Manuel González-Guerrero
Email: manuel.gonzalez@upm.es

Viviana Escudero
Email: viviana.escudero@upm.es

Received: 27 June 2023

Accepted: 3 October 2023

New Phytologist (2024) 241: 793–810
doi: 10.1111/nph.19360

Key words: copper, copper transport, metallochaperone, nitrogen fixation, nodulation.

- Cu⁺-chaperones are a diverse group of proteins that allocate Cu⁺ ions to specific copper proteins, creating different copper pools targeted to specific physiological processes.
- Symbiotic nitrogen fixation carried out in legume root nodules indirectly requires relatively large amounts of copper, for example for energy delivery via respiration, for which targeted copper delivery systems would be required.
- MtNCC1 is a nodule-specific Cu⁺-chaperone encoded in the *Medicago truncatula* genome, with a N-terminus Atx1-like domain that can bind Cu⁺ with picomolar affinities. MtNCC1 is able to interact with nodule-specific Cu⁺-importer MtCOPT1. MtNCC1 is expressed primarily from the late infection zone to the early fixation zone and is located in the cytosol, associated with plasma and symbiosome membranes, and within nuclei. Consistent with its key role in nitrogen fixation, *ncc1* mutants have a severe reduction in nitrogenase activity and a 50% reduction in copper-dependent cytochrome c oxidase activity.
- A subset of the copper proteome is also affected in the *ncc1* mutant nodules. Many of these proteins can be pulled down when using a Cu⁺-loaded N-terminal MtNCC1 moiety as a bait, indicating a role in nodule copper homeostasis and in copper-dependent physiological processes. Overall, these data suggest a pleiotropic role of MtNCC1 in copper delivery for symbiotic nitrogen fixation.

Introduction

Copper is an essential nutrient for plants (Marschner, 2011). It is involved in key physiological processes such as photosynthesis, respiration, ethylene signalling, or free radical control, among many others (Andresen *et al.*, 2018). This versatile use of copper is largely based on its ability to transition between two redox states (Cu⁺ and Cu²⁺) in physiological conditions (Burkhead *et al.*, 2009). However, this property also underlies the potential toxicity of cytosolic copper, when the concentration of copper exceeds the capacity of the cell to avoid cytotoxic interactions (Küpper & Andresen, 2016). One suggested mechanism of toxicity is the nonenzymatic catalysis of Fenton-style reactions producing damaging free radicals (Goldstein *et al.*, 1993). Furthermore, excess copper in the cytosol can displace other essential transition metals from the active site of metalloproteins (Küpper *et al.*, 1996, 2002; Macomber & Imlay, 2009). As a result, and to prevent copper damage to the cell structures, the

‘free’, hydrated concentrations of copper in the cytosol are maintained at extremely low levels, less than one ion per cell (Changella, 2003). This is achieved by the coordinated action of small, copper-binding molecules, as well as proteins known as Cu⁺-chaperones (Robinson & Winge, 2010; Flis *et al.*, 2016).

The role of Cu⁺-chaperones is to deliver copper to different copper proteins, protecting the cell from copper toxicity (Lin *et al.*, 1997; Wong *et al.*, 2000). Cu⁺-chaperones bind Cu⁺ with picomolar (pM) to femtomolar (fM) affinity (Rae *et al.*, 1999; Palumaa *et al.*, 2004), which prevents unspecific copper release before docking with a compatible protein. This means that metalation is not simply the result of relative copper-binding affinities, but also of the specific protein–protein interaction between donor and acceptor proteins. Consequently, different copper pools are created based on the ability of each protein to interact and exchange copper with one or another Cu⁺-chaperone. *Saccharomyces cerevisiae* has at least three of these pools: the secretory pathway that receives copper from Atx1 (Lin *et al.*, 1997);

COX17, the Cu⁺-chaperone for cytochrome *c* oxidase (Palumaa *et al.*, 2004); and the Cu, Zn superoxide dismutase that gets it from CCS (Rae *et al.*, 1999). Multicellular organisms are expected to have a larger number of such proteins, which are related in structure but serve a diversity of functions. Plants have at least a CCS orthologue (Chu *et al.*, 2005), two Cu⁺-chaperones driving copper to cytochrome *c* oxidase (Attallah *et al.*, 2011), another in the inter-envelope space of the chloroplasts (Blaby-Haas *et al.*, 2014), and three ATX1 orthologues with the characteristic Cu⁺-binding CXXC motive: ATX1 (Shin *et al.*, 2012), CCP (Chai *et al.*, 2020) and CCH (Mira *et al.*, 2001), the later with a C-terminal domain of unknown function. This multiplicity of Cu⁺-chaperones hints not only at the existence of different copper pools, but also at their specialized roles in plant physiology. For instance, ATX1 seems to be involved in buffering through copper deficiency or excess (Shin *et al.*, 2012), CCH has been proposed to be involved in recovering copper during leave senescence (Mira *et al.*, 2001), and CCP plays a role in plant immunity (Chai *et al.*, 2020). Therefore, it should be expected that other, new Cu⁺-chaperones are associated with other copper-dependent processes.

While leaves are the main copper sink in most plants during vegetative growth, legumes have a second, major copper sink in their root nodules (Johnston *et al.*, 2001; Senovilla *et al.*, 2018). After the exchange of specific signals between legumes and a group of bacteria known as rhizobia, cells in the root cortex, pericycle and endodermis proliferate to produce nodules (Downie, 2014; Xiao *et al.*, 2014). Concomitant to nodule development, rhizobia penetrate and colonize nodule cells. Surrounded by the plant-derived symbiosome membrane, rhizobia differentiate into bacteroids that synthesize nitrogenase to fix nitrogen. This developmental process can be easily followed in indeterminate-type nodules, such as those in pea or in *Medicago truncatula*. Indeterminate nodules maintain their apical meristem over time, leading to a spatial–temporal gradient. As a result, four developmental zones can be observed in these nodules: the apical meristem (zone I), the infection-differentiation zone (zone II), an interzone where oxygen levels drop to prevent nitrogenase inhibition, so that nitrogen fixation can occur in the fixation zone of the nodule (zone III), and a senescent zone (zone IV) in older nodules (Vasse *et al.*, 1990). In exchange for this fixed nitrogen, the host plant provides photosynthates and mineral nutrients, including copper (Udvardi & Poole, 2013; Senovilla *et al.*, 2018).

Legume nodules accumulate high levels of copper (*c.* 50 µg g⁻¹; Senovilla *et al.*, 2018), evidencing an important role for this nutrient in nodule development and/or symbiotic nitrogen fixation. Further evidence is provided by the existence of a nodule-specific copper uptake transporter, MtCOPT1, that is required for optimal nitrogen fixation and cytochrome oxidase activity of bacteroids (Senovilla *et al.*, 2018). Therefore, it should be expected that specific mechanisms are in place to ensure copper allocation to enzymes involved in symbiotic nitrogen fixation in legume nodules, and that this is achieved via dedicated Cu⁺-chaperones. This manuscript provides data supporting this hypothesis, as it reports that

Medtr3g067750 is a nodule-specific Cu⁺-chaperone (NCC) that is essential for symbiotic nitrogen fixation.

Materials and Methods

Biological materials and growth conditions

Medicago truncatula Gaertner R108 seeds were scarified in pure H₂SO₄ for 7.5 min. Then, they were washed with cold water and sterilized with 50% bleach for 1.5 min and imbibed in sterile water in darkness overnight. On the following day, seeds were placed on water-agar plates for 48 h at 4°C and then allowed to germinate at 22°C for 24 h. Seedlings were planted in sterile perlite pots and inoculated with *Sinorhizobium meliloti* 2011 or *S. meliloti* 2011 transformed with pHc60 (Cheng & Walker, 1998), as indicated. Plants were grown in a glasshouse at 16 h : 8 h, light : dark and 22°C and watered with Jenner's solution or water every 2 d, alternatively (Brito *et al.*, 1994). Nodules were collected at 28 d postinoculation (dpi). Noninoculated plants were cultivated in similar conditions, but they were watered every 2 wk with Jenner's solution supplemented with 2 mM NH₄NO₃. For hairy-root transformations, *M. truncatula* seedlings were infected with *Agrobacterium rhizogenes* ARqual carrying the appropriate binary vector as described (Boisson-Dernier *et al.*, 2001). In agroinfiltration experiments, *Nicotiana benthamiana* (tobacco) leaves were infected with the plasmid constructs in *A. tumefaciens* GV3101 (Deblaere *et al.*, 1985). Tobacco plants were grown under the same conditions as *M. truncatula*.

For yeast complementation assays, *Saccharomyces cerevisiae* strain Δ*atx1* and its parental strain BY4741 (MAT_a *his3Δ 1 leu2Δ 0 met15Δ 0 ura3Δ 0*) were purchased from the Yeast Knockout Collection (GE Dharmacon, Lafayette, CO, USA). Yeasts were grown in yeast peptone dextrose (YPD) or in synthetic dextrose (SD) media supplemented with 2% glucose (Sherman *et al.*, 1983). Phenotypic characterization was performed in yeast peptone ethanol glycerol (YPEG) medium (Li & Kaplan, 2001).

For protein purification, *Escherichia coli* BL21 (DE3) pLysS (Wood, 1996) (*E. coli* str. B F-ompT gal dcm lon hsdSB (*r_B-m_B*) λ(DE3 (*lacI lacUV5-T7p07 ind1 sam7 nin5*)) (*malB*⁺)_{K-12} (λ^S) pLysS (T7p20 ori_{p15A}) (Cm^R) was used to produce the required amount of protein.

Quantitative real-time RT-PCR

RNA isolation and cDNA synthesis were carried out as described previously (Tejada-Jiménez *et al.*, 2015). Gene expression was studied by quantitative real-time RT-PCR (9700, Applied Biosystems) with primers indicated in Supporting Information Table S1 and normalized to the *M. truncatula* Ubiquitin carboxy-terminal hydrolase gene (*Medtr4g077320*). Real-time cycler conditions have been described previously (González-Guerrero *et al.*, 2010). Determinations were performed with RNA extracted from three independent biological samples, with the threshold cycle determined in triplicate. The relative levels of transcription were determined with the 2^{-ΔC_t} method.

Yeast complementation assays

MtNCC1 and *MtNCC1_{1–78}* cDNAs were cloned into the yeast expression vector pDR196, between *PstI* and *XbaI* restriction sites, by homologous recombination in yeast (primers indicated in Table S1). For yeast transformation, a lithium acetate-based method was used as described (Schiestl & Gietz, 1989). Transformants were selected in SD medium by uracil autotrophy. Phenotypic analysis of yeast transformants was done on YPEG plates (Li & Kaplan, 2001).

Protein expression and purification

MtNCC1_{1–78} was obtained by PCR using *MtNCC1* cDNA as the template (primers indicated in Table S1). The resulting cDNA was cloned between *NdeI* and *BamHI* restriction sites in a modified version of pET16b (courtesy of Dr. Luis Rubio). This plasmid adds two N-terminal streptavidin (N-Twin-Strep (N-TS)) tag sequences. Protein expression was induced for 3 h at 37°C by the addition of 1 mM IPTG to *E. coli* BL21 cells (Wood, 1996). Cells expressing soluble *MtNCC1_{1–78}* were disrupted in 100 mM Tris (pH 8.0), 150 mM NaCl (buffer W) using a French press. Homogenates were centrifuged at 54 000 g for 1 h. The protein was purified with a Strep-Tactin XT 4Flow high-capacity column (IBA Lifesciences) and stored in 10% glycerol in buffer W at –80°C. Protein quantification was performed in accordance with the Bradford assay (Bradford, 1976).

Cu⁺-binding affinity

Proteins' *K_a* value was obtained by using a competition assay with BCA followed by colorimetric determination of the BCA₂·Cu⁺ complex at 360 nm. *K_a* was determined by titrating with Cu⁺ in a solution of 20 μM BCA, 100 μM *MtNCC1_{1–78}* in 50 mM HEPES (pH 7.5), 200 mM NaCl and 200 μM ascorbate (buffer H). The BCA₂·Cu⁺ molar extinction coefficient, ε₃₆₀ = 20 600 cm^{–1} M^{–1}, was determined by titrating μM Cu⁺ with 0–10 μM BCA in buffer H. Free metal concentrations were calculated from $K_{BCA} = [BCA_2 \cdot Cu^+]/[BCA_{free}]^2[Cu^+_{free}]$, where *K_{BCA}* is the association constant for BCA₂·Cu⁺ (4.60×10^{14} M^{–2}; Yatsunyk & Rosenzweig, 2007; González-Guerrero & Argüello, 2008). The *K_a* values were calculated by using $\nu = [Cu^+_{free}]^n K_a / (1 + K_a [Cu^+_{free}]^n)$, where *ν* is the molar ratio of metal bound to protein and *n* is the number of metal-binding sites. Reported errors for *K_a* and *n* are asymptotic standard errors provided by the fitting software (ORIGIN; OriginLab, Northampton, MA, USA).

GUS staining

MtNCC1 promoter (*MtNCC1p*; 2-kb upstream of the *MtNCC1* start codon) was amplified using the primers indicated in Table S1, then cloned into pDONR207 (Invitrogen) and transferred to pGWB3 vector containing the *GUS* gene (Nakagawa *et al.*, 2007), using Gateway Cloning technology (Invitrogen). *M. truncatula* hairy-root transformation was carried out as described previously. Transformed seedlings were planted

in sterile perlite pots and inoculated with *S. meliloti* 2011. GUS activity was measured in nodules of 28 dpi plants as described (Vernoud *et al.*, 2007).

Immunolocalization

A DNA fragment containing the full-length *MtNCC1* genomic region, and the *MtNCC1p* was cloned into the pGWB13 (Nakagawa *et al.*, 2007) by Gateway technology (Invitrogen). This vector fuses 3 HA epitopes in the C-terminus of the protein. *M. truncatula* hairy-root transformation was carried out as described previously (Boisson-Dernier *et al.*, 2001). Transformed seedlings were planted in sterile perlite pots and inoculated with *S. meliloti* 2011 integrating the pHc60 vector that constitutively expresses GFP. Twenty-eight dpi nodules were collected and fixed in 4% (w/v) paraformaldehyde and 2.5% (w/v) sucrose in phosphate-buffered saline (PBS) at 4°C overnight. The next day, nodules were washed in PBS, and 100 μm sections were generated with a Vibratome 1000 plus (Vibratome, St Louis, MO, USA). Then, the sections were dehydrated using a methanol series (30, 50, 70 and 100% (v/v) in PBS) for 5 min and then rehydrated. Cell walls were permeabilized with 4% (w/v) cellulase in PBS for 1 h at room temperature and treated with 0.1% (v/v) Tween 20 in PBS for 15 min. The sections were blocked with 5% (w/v) bovine serum albumin (BSA) in PBS and incubated then with an anti-HA mouse monoclonal antibody (Sigma) for 2 h at room temperature. After washing the primary antibody, the sections were incubated with an Alexa594-conjugated anti-mouse rabbit monoclonal antibody (Sigma) for 1 h at room temperature. After removing the unbound secondary antibody, DAPI (4',6'-diamidino-2-phenylindole) was used to stain the DNA. Images were acquired with a confocal laser-scanning microscope (Leica SP8; Leica, Wetzlar, Germany) using excitation lights at 488 nm for GFP and at 561 nm for Alexa 594.

For gold-immunolocalization, 28 dpi nodules were collected and fixed in 1% formaldehyde and 0.5% glutaraldehyde in 50 mM potassium phosphate (pH 7.4) for 2 h. The fixation solution was renewed and incubated for an additional 1.5 h. Samples were washed in 50 mM potassium phosphate (pH 7.4) three times for 30 min and three times for 10 min. Nodules were dehydrated by incubating with ethanol dilution series of 30, 50, 70 and 90% for 10 min, 96% for 30 min and 100% for 1 h. Samples were incubated with a series of ethanol and LR-white resin (London Resin Co. Ltd, Reading, UK) dilutions: 1 : 3 for 3 h, 1 : 1 overnight and 3 : 1 for 3 h, and left in LR-white resin for 48 h. All incubations were done at 4°C. Nodules were placed in gelatine capsules previously filled with LR-white resin and polymerized at 60°C for 24 h. Ultra-thin sections were cut at Centro Nacional de Microscopía Electrónica (Universidad Complutense de Madrid, Spain) with Reichert Ultracut S-ultramicrotome fitted with a diamond knife. The sections were blocked in 2% BSA in PBS for 30 min. An anti-HA rabbit monoclonal antibody (Sigma) was used (dilution 1 : 20 in PBS) as primary antibody. The samples were washed 10 times in PBS for 2 min. As a secondary antibody, 1 : 150 dilution in PBS of antirabbit goat antibody conjugated to a 15 nm gold particle (BBI Solutions, Berlin, Germany) was used. Incubation was performed

for 1 h. The sections were washed 10 times with PBS for 2 min and 15 times with water for 2 min, stained with 2% uranyl acetate and visualized in a JEM 1400 electron microscope at 80 kV.

Acetylene reduction assay

Nitrogenase activity was determined by the acetylene reduction assay (Hardy *et al.*, 1968). Nitrogen fixation was analysed in mutant and control plants at 28 dpi in 30-ml vials fitted with rubber stoppers. Each tube contained one independently transformed plant. Three ml of air inside the vial was replaced by 3 ml of acetylene, and then, they were incubated at room temperature for 30 min. Gas samples (0.5 ml) were analysed in a Shimadzu GC-8A gas chromatograph fitted with a Porapak N column. The amount of ethylene produced was determined by measuring the height of the ethylene peak relative to the background. After measurements, nodules were collected from roots for weighing.

Cytochrome oxidase activity

Nodules from 28 dpi plants were collected and used for bacteroid isolation, as described by Brito *et al.* (1994) with modifications. Nodules from 50 plants (0.1–0.3 g nodules) were pooled together and crushed with 33% (w/w) of polyvinylpyrrolidone and 1 ml of extraction buffer (38 mM K₂HPO₄, 24 mM KH₂PO₄ and 2.4 mM MgCl₂). Three consecutive centrifugations were performed with the supernatant of the previous one, two at 1000 **g** (1 and 5 min) and a final one at 5000 **g** for 10 min. The final pellet was resuspended in 500 µl of resuspension buffer (50 mM HEPES, 200 mM NaCl pH 7). Cytochrome oxidase activity was determined by N,N,N',N'-tetramethyl-p-phenylenediamine (TMPD) oxidation assay. The reaction was started by adding TMPD to the bacteroid sample at a final concentration of 2.7 mM. To obtain the reaction kinetics, each sample was measured at OD₅₂₀ every 10 s for 3 min. To measure protein content and to calculate specific activity, the bacteroid suspension was lysed in 10% SDS at 90°C for 5 min. The amount of protein was determined with the Pierce™ BCA Protein Assay Kit (Thermo Fisher Scientific, Waltham, MA, USA).

Metal content determination

To determine metal content, inductively coupled plasma–mass spectrometry (ICP-MS) was performed for three independent sets of 28 dpi roots, shoots and nodules pooled from 10 plants. Elemental analysis with ICP-MS was carried out at the Unit of Metal Analysis from the Scientific and Technology Centre, Universidad de Barcelona (Spain). These samples were treated with HNO₃, H₂O₂ and HF in a Teflon reactor at 90°C. The resulting homogenates were diluted with deionized water. Final volumes were calculated by weight and weight : volume ratios. In parallel, samples were digested with three blanks. Metal determination was carried out in an Agilent 7500cw (Agilent, Santa Clara, CA, USA) with standard instrument conditions. Calibration and internal standardization for obtaining the calibration curve were done with five solutions prepared from certified NIST standards.

Metalloproteomics

Metalloproteomic analyses were performed on 150 28 dpi nodules from wild-type (WT) or *ncc1* plants. Soluble and membrane proteins were extracted from the nodules as described by Andresen *et al.* (2016). Afterwards, proteins were separated by size exclusion chromatography coupled to ICP-sfMS as described (Küpper *et al.*, 2019). Briefly, two Superdex Increase 200 10 × 300 mm and one Superdex Increase 75 10 × 300 mm size exclusion columns were used to separate the nodule protein extracts in 150 mM ammonium bicarbonate buffer with 0.2 mM DDM. Detection was achieved with a customized sector field ICP-MS (Element XR-2 with jet interface and desolvating injection; Thermo Fisher Scientific), and a diode array detector coupled to a metal-free HPLC system (Azury System, Knauer, Germany). Metal-EDTA complexes in the same buffer as the protein extracts were used to calibrate concentration determination. A gel filtration calibration standard (Bio-Rad with added PABA) was used to determine size and molecular weight. Calibration of metal concentrations in the ICP-sfMS chromatograms was performed as described in Küpper *et al.* (2019). Proteins were identified in the Proteomic Unit of Universidad Complutense de Madrid (Spain).

Proteomics

Proteomic analyses were performed in the Proteomics Unit of Complutense University of Madrid, a member of Proteored. Samples were lyophilized and resuspended in 100 µl of 25 mM ammonium bicarbonate buffer and quantified. Proteins were reduced in 10 mM DTT at 56°C for 60 min and subsequently alkylated in 25 mM iodoacetamide for 60 min in darkness at room temperature. Samples were digested with Trypsine/LysC protease mix (Pierce; Thermo Fisher Scientific) at a 1 : 30 (w/w) ratio overnight at 37°C. Desalted and concentrated peptides were lyophilized and reconstituted in 15 µl 2% acetonitrile and 0.1% formic acid. One µg of peptides from each sample were analysed by liquid nano-chromatography (Vanquish Neo; Thermo Fisher Scientific) coupled to a high-resolution mass spectrometer (Q-Exactive HF; Thermo Fisher Scientific). The acquired MS/MS spectra were analysed using Proteome Discoverer 3 (Thermo Fisher Scientific) using Mascot 2.8 search engine and the databases SwissProt, *M. truncatula*, *S. meliloti* downloaded from Uniprot. ‘Correctly’ identified proteins are those that have a false discovery rate (FDR) below 1% and at least on single peptide identified with high confidence (above 99%).

Pull-down assay

Twenty-eight grams of fresh *M. truncatula* R108 nodules (from c. 2,500 plants) were homogenized manually with a mortar and pestle. The homogenate was centrifuged at 20 000 **g** 4°C for 30 min. To separate soluble from membrane proteins, the supernatant ('cell free' extract) was centrifuged at 100 000 **g** 4°C for 1 h. The resulting supernatant containing soluble proteins was loaded in Strep-Tactin XT 4Flow High-Capacity column (IBA Lifesciences, Göttingen, Germany) previously saturated with

N-TS-MtNCC_{1–78}·Cu⁺. Co-eluting proteins were identified by liquid chromatography–mass spectrometry (LC–MS/MS) at the Proteomic Unit of the Universidad Complutense de Madrid (Spain).

Bimolecular fluorescence complementation

MtNCC1 or *MtNCC1_{1–78}* CDSs were fused at the N-terminus to the N-fragment of yellow fluorescence protein (YFP) in the Gateway vector pNXGW (Kim *et al.*, 2009). The CDS of MtNCC1 candidate interactors were fused to the C-fragment of cyan fluorescence protein (CFP) at both N- and C-terminus in the Gateway vectors pCXGW and pXCGW (Kim *et al.*, 2009), respectively. Primers for cloning are indicated in Table S1. These constructs were introduced into *A. tumefaciens* GV3101 (Deblaere *et al.*, 1985). *N. benthamiana* leaves were infiltrated as described previously (Senovilla *et al.*, 2018). Leaves were examined after 3 d by confocal laser-scanning microscopy (LSM 880; Zeiss) with excitation light of 488 nm for GFP.

Cu⁺-transfer assays

Freshly Cu⁺-loaded Twin Strep-tagged MtNCC_{1–78} was incubated with Strep-Tactin XT 4Flow high-capacity resin in a column for 10 min at room temperature with gentle agitation. The column was washed with 10 volumes of freshly made 10 mM ascorbate in 50 mM HEPES (pH 7.5) and 200 mM NaCl (Buffer T). 10× Histidine-tagged (His₁₀) putative universal stress protein A was loaded onto this resin with MtNCC_{1–78} and incubated for 10 min at room temperature with gentle agitation to initiate Cu⁺-exchange. The column was washed again with 10 volumes of freshly made 10 mM ascorbate in buffer T, and the bound proteins were eluted with 50 mM biotin in buffer T. Copper and protein concentrations were determined in all fractions by competition assays with BCA (Brenner & Harris, 1995) and Bradford assay (Bradford, 1976), respectively. Protein content in selected fractions was analysed by SDS-PAGE using 15% acrylamide/bisacrylamide (37.5 : 1) gels and visualized by Coomassie Brilliant Blue staining. For immunoblot analysis, proteins were transferred to nitrocellulose membranes for 45 min at 20 V using a Transfer-Blot® Semi Dry system (Bio-Rad). Immunoblot analyses were carried out with antibodies against Strep (Strep-Tactin HRP conjugate, IBA) and His (α -His primary monoclonal antibody, Santacruz) tags using a 1 : 8000 and 1 : 1000 dilution, respectively. For His₁₀ immunoblot, a horseradish peroxidase-conjugated anti-mouse antibody (Invitrogen) diluted 1 : 1000 was used as a secondary antibody. Chemiluminescent detection was carried out according to Pierce ECL Western Blotting Substrate Kit's instructions (Thermo Fisher Scientific) and developed in an iBright FL1000 Imaging System (Thermo Fisher Scientific).

Statistical tests

Data were analysed using Student's unpaired *t*-test to calculate statistical significance of observed differences. Test results with *P*-values < 0.05 were considered as statistically significant.

Results

MtNCC1 is a Cu⁺-chaperone

To identify candidate Cu⁺-chaperones in *Arabidopsis thaliana* and *M. truncatula*, we collected those sequences annotated as such, as well as those annotated as metal-binding domain proteins or HIPP, removing those that did not contain a CXXC Cu⁺-binding motive. Over 30 different candidates were identified in the genomes of these two plant species (Fig. S1; Methods S1). A second filter was applied to remove those that have an extra-binding amino acid (typically D/E) flanking the Cys in the CXXC domain, as they confer increased affinity for divalent metal (Zn²⁺, Cu²⁺ and Ni²⁺) binding rather than Cu⁺ (Eren *et al.*, 2007; Tehseen *et al.*, 2010). Within *M. truncatula*, there was a nodule-specific candidate, *Medtr3g067750* (NCC1, for Nodule-specific Cu⁺-Chaperone 1), as indicated by the available transcriptomic databases (Fig. S2). This expression pattern was validated by qRT-PCR analyses (Fig. 1a). However, MtNCC1 was not the only candidate Cu⁺-chaperone expressed in nodules (Table S2). Protein modelling showed the existence of two different protein domains in MtNCC1: a N-terminal Atx1-like domain comprised of the first 78 amino acids (MtNCC_{1–78}) that included the CXXC motif, and a C-terminal, intrinsically disordered region, with a D-rich motif (Fig. 1b).

Yeast complementation assays of the yeast *atx1* mutant were used to determine whether the candidate protein above could rescue the copper-homeostasis defect of the yeast Cu⁺-chaperone Atx1. This strain cannot grow in nonfermentative carbon sources (Dimmer *et al.*, 2002; Soma *et al.*, 2018). However, *atx1* showed WT growth when expressing *MtNCC1* or *MtNCC1_{1–78}* (Fig. 1c). To further determine whether MtNCC1 could work as a Cu⁺-chaperone, Strep-tagged MtNCC_{1–78} was purified from *Escherichia coli* (Fig. S3) and used to determine Cu⁺-binding stoichiometry and affinity. As expected for an Atx1-like chaperone, MtNCC_{1–78} bound one Cu⁺ per molecule with an affinity constant of 2.45 pM⁻¹ (Fig. 1d). A similar stoichiometry was observed after incubating MtNCC_{1–78} with a 10-fold molar excess of Cu⁺ and removing the unbound metal (Fig. S4; Methods S1). Consistent with a role as a Cu⁺-chaperone, bimolecular fluorescence complementation (BiFC) studies showed the MtNCC1 interacted with nodule-specific Cu⁺ importer MtCOPT1 in the plasma membrane (Fig. 2). No signal was observed when MtNCC1 was co-transformed with the empty vectors or with one containing the *gus* gene (Fig. S5).

MtNCC1 is located in the cytosol and nucleus of nodule cells

To determine whether MtNCC1 was produced in the nodule, promoter-GUS fusions were transformed in *M. truncatula* plants. As shown in Fig. 3a, *MtNCC1* was highly expressed in the infection-differentiation zone (ZII), interzone (IZ) and early fixation zone (ZIII) of the nodules, although lower expression levels could be found in older fixation zone areas. This expression pattern is consistent with the transcriptomic data obtained from

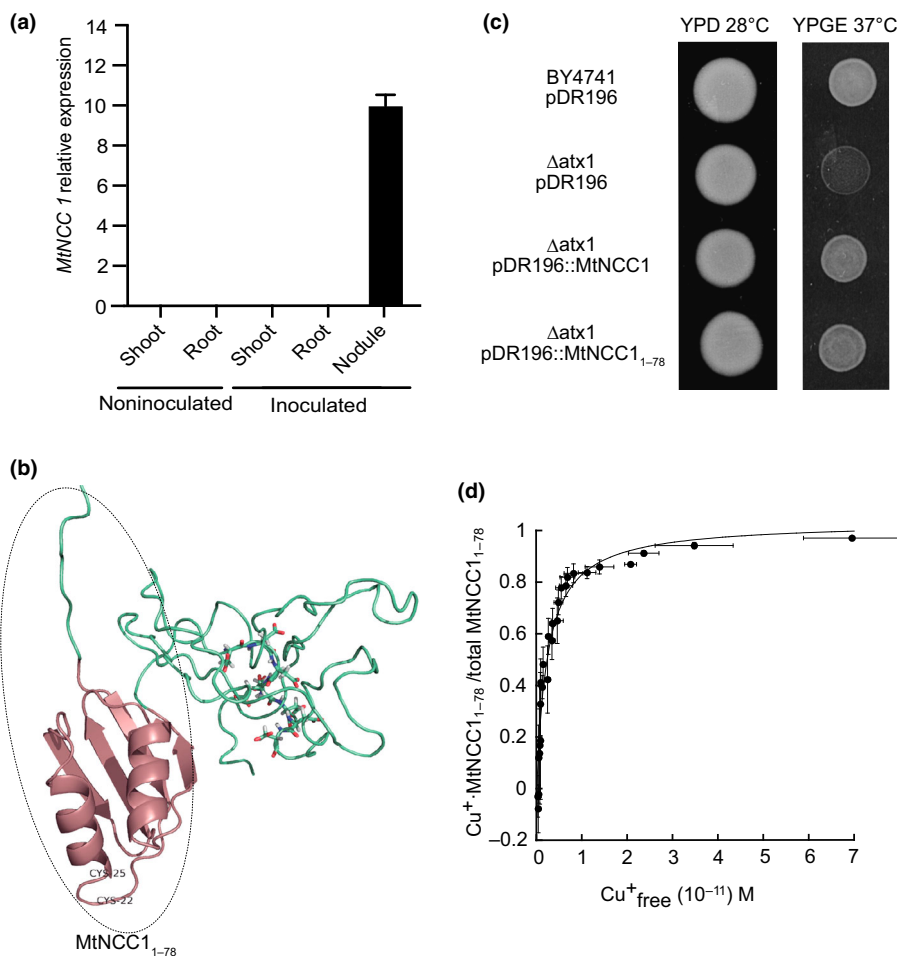


Fig. 1 MtNCC1 is a nodule-specific Cu⁺-chaperone. (a) MtNCC1 expression in *Sinorhizobium meliloti*-inoculated (roots, shoots and nodules) and noninoculated (roots and shoots) *Medicago truncatula* plants relative to standard gene *Ubiquitin carboxyl-terminal hydrolase*. Data are the mean \pm SE of three independent experiments with five pooled plants. (b) Predicted structure of MtNCC1 using iTasser and Alpha-fold. The classical Atx1-like domain is indicated in pink, with the two conserved Cu⁺-binding cysteines (C22 and 25). The aspartate-rich region in the C-terminal domain is indicated with wireframes. Dotted line surrounds the MtNCC1_{1–78} region. (c) Yeast complementation of the atx1 phenotype. Parental strain BY4741 was transformed with empty pDR196 vector, while the Δatx1 mutant NCC1 was transformed with empty pDR196 or containing MtNCC1 or MtNCC1_{1–78}. (d) Cu⁺ binding to MtNCC1_{1–78} determined in competition assays with BCA. The data were fit using $n = 1.03 \pm 0.04$ Cu⁺ per protein and $K_a = 2.45 \pm 0.34$ pM⁻¹. Data are the mean \pm SE ($n = 3$).

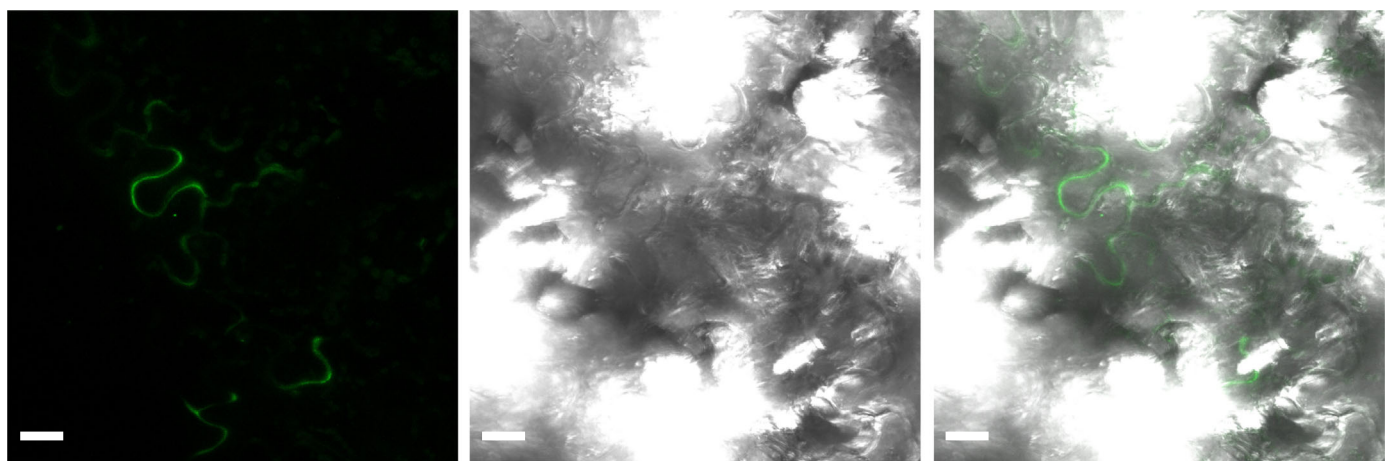


Fig. 2 Bimolecular fluorescent complementation assay of MtNCC1 and MtCOPT1 interaction. Transient co-expression of MtNCC1 in pNXGW and MtCOPT1 in pCXGW in *Nicotiana benthamiana* leaf cells 3 d-postagroinfiltration. Left panel corresponds to the fluorescent signal resulting from the interaction between MtNCC1 MtCOPT1 (green); central panel, transillumination; right panel, overlaid fluorescent image and transillumination images. Bars, 20 μ m.

laser-captured micro-dissected cells in the Symbimics database (Fig. 3b). Moreover, immunolocalization of hemagglutinin epitope (HA)-tagged MtNCC1 showed a similar distribution pattern (Fig. 3c). Higher magnification images of nodule cells showed

MtNCC1-HA in the cytoplasm and in the nuclei in infected and uninfected cells (Fig. 3d). This distribution pattern was not observed in un-transformed plants (Fig. S6). Additionally, MtNCC1_{1–78}-HA had the same distribution pattern (Fig. S7).

Electron-microscopy images using a gold-conjugated antibody revealed that MtNCC1-HA was found in the cytosol, as well as associated with the plasma and symbosome membranes (Fig. 3e).

MtNCC1 is required for symbiotic nitrogen fixation

To determine the physiological role of MtNCC1, an insertional *ncc1* mutant was obtained from a *M. truncatula* *Tnt1* mutant collection. This line had an insertion in position +1044 that led to loss of *MtNCC1* expression (Fig. 4a). As expected, the mutant line did not present any apparent phenotype under nonsymbiotic conditions (Fig. S8), but showed a significantly reduced growth and biomass production in symbiosis (Fig. 4b,c). No significant changes in nodule development, zonation, or in bacteroid size were observed compared with WT plants (Fig. S9; Methods S1). The nitrogenase activity in *ncc1* plants was severely reduced (Figs 4d, S10). Analyses of *MtNCC1* WT *ncc1* segregants suggested that no additional *Tnt1* insertions elsewhere in the genome could explain these phenotypical effects (Fig. 5). Furthermore, growth and nitrogenase activity were restored by introducing a WT copy of *MtNCC1* into the mutant line (Fig. 4b–d). Finally, cytochrome oxidase activity was significantly reduced in bacteroids, but to a much lower extent than the nitrogenase activity (Fig. 4e).

MtNCC1 mutation affects a subset of the copper proteome

Consistent with the role of MtNCC1 in copper metabolism, increasing copper concentrations by 10-fold in the nutrient solution was sufficient to restore WT growth and nitrogenase activity in *ncc1* plants (Fig. 5). However, overall copper concentrations in the analysed plant organs (roots, shoots and nodules) were not significantly altered in *ncc1* plants when watered with standard or copper-supplemented nutrient solutions (Fig. S11a,b). Iron levels were not affected either (Fig. S11c,d). Importantly, metalloproteomic analyses on nodule soluble protein extracts from WT and *ncc1* nodules showed reduced copper contents in a subset of the proteome (Fig. 6a). The largest differences were found c. 110 and 60 kDa. As this was a separation only by SEC, the copper proteins only represented a small proportion of the total proteins eluting during the times when a maximal difference between the WT and *ncc1* samples was observed. This becomes clear when looking at the profiles of other metals at the same time and comparing the UV/VIS spectra with the metal chromatograms (regions of interest in Fig. 6b,c, complete time range in Fig. S12).

Therefore, although copper-binding proteins were affected, the total number of proteins contained in two fractions (chosen in the MW ranges of max. differences in copper, Fig. 6a) in WT and *ncc1* nodules remained largely the same (Tables S3, S4); only 70 out of 1529 proteins in fraction 1 and 12 out of 1900 proteins in fraction 2 missing in *ncc1* compared with WT. None of the top 10 detected proteins of these differentially expressed proteins have a known role in copper homeostasis (Table 1). However, for the most abundant among them, S-adenosylmethionine synthase,

it has previously been shown that it was up-regulated in response to copper in relation to ethylene synthesis (Zhang *et al.*, 2018). Furthermore, heat-shock proteins are generally known to bind copper with extremely high (picomolar) affinity (Ahmad *et al.*, 2008). Similarly, experimental evidence supports copper-dependent modulation of the activity of a putative GTPase and a glyceraldehyde 3-phosphate dehydrogenase as those listed in Table 1 (Gao *et al.*, 2005; Chong & Ho, 2019). Looking at the entire HPLC-ICPs-fMS chromatograms in more detail (Fig. S12) reveals additional minor changes in the metalloproteome that would result from the cross-talk between copper homeostasis and that of other elements. Analysing these changes would be a topic for another study.

In a further attempt to identify proteins that would accept Cu⁺ by interacting with MtNCC1, Cu⁺-loaded MtNCC1_{1–78} (MtNCC1_{1–78}·Cu⁺) was used as a bait for pull-down assays. To ensure that the identified proteins were those that specifically interacted with MtNCC1_{1–78}·Cu⁺ and not with the resin, control pull-down assays in which no bait was bound to the resin were done in parallel. The proteins specifically retained by MtNCC1_{1–78}·Cu⁺ are indicated in Table S5. Approximately one-third of these proteins were also present in the selected fractions from the metalloproteomic analyses (Table S6), and mostly, they are putatively involved in D-gluconate catabolism, S-adenosylmethione (SAM) cycle, endoplasmatic reticulum unfolded protein response and protein import into the nucleus. Among them, known proteins using copper were identified. These included various heat-shock proteins, but also galactose oxidase as one of the best and longest-known enzymes with copper in its active site (Hamilton *et al.*, 1973). Furthermore, some contained the Cu⁺-binding motif CXXC, such as SAM synthases or protein disulphide isomerase. The latter class of enzymes is known to have copper in its active site (Schultz *et al.*, 1999; Narindrasorasak *et al.*, 2003). Others (adenosyl-homocysteinase or putative universal stress protein A, for instance) had two cysteines close enough to bind Cu⁺ according to the Alpha-fold predicted structure. Finally, the list contains proteins where copper is not natively bound but where copper binding is known in an inhibitory way. Some of them, where it was particularly clear, are labelled in Tables 1, S6.

To validate some of these putative interactions, BiFC studies were carried out in agroinfiltrated tobacco leaves expressing MtNCC1_{1–78} together with randomly selected candidates identified in the pull-down experiments. As shown in Fig. 7, MtNCC1_{1–78} interacted with thioredoxin-dependent peroxiredoxin (*Medtr7g105830*), CXXC-containing SAM synthase (*Medtr2g046710*), nodule-specific putative universal stress protein- (USP) A (*Medtr1g088640*) with a predicted Cu⁺-binding site according to Alpha-fold (Fig. S13) and nodule-specific pathogenesis-related protein (*Medtr2g076010*). No signal was observed when MtNCC1_{1–78} was expressed in leaves infiltrated with the empty vectors or with a GUS-expressing one (Fig. S14). The putative USP-A was purified (Fig. S15; Methods S1) to determine its Cu⁺-binding affinity constant and its capacity to accept Cu⁺ from MtNCC1_{1–78}. The putative

Cu^+ -acceptor could bind one Cu^+ per protein with an affinity of 12.67 pM^{-1} (Fig. 8a). Incubation of Cu^+ -loaded twin strep-tagged NCC1_{1–78} with His₁₀-tagged apo-putative USP-A and separation in a strep-binding resin resulted in copurification of USP-A together with NCC1_{1–78} (Fig. 8b). Furthermore, in

this interaction, the putative USP-A was able to accept the Cu^+ provided by MtNCC1_{1–78} (Fig. 8c). This Cu^+ -transfer occurred only when protein–protein interaction was possible, as no Cu^+ was exchanged when the two proteins were separated by a dialysis membrane (Fig. S8d).

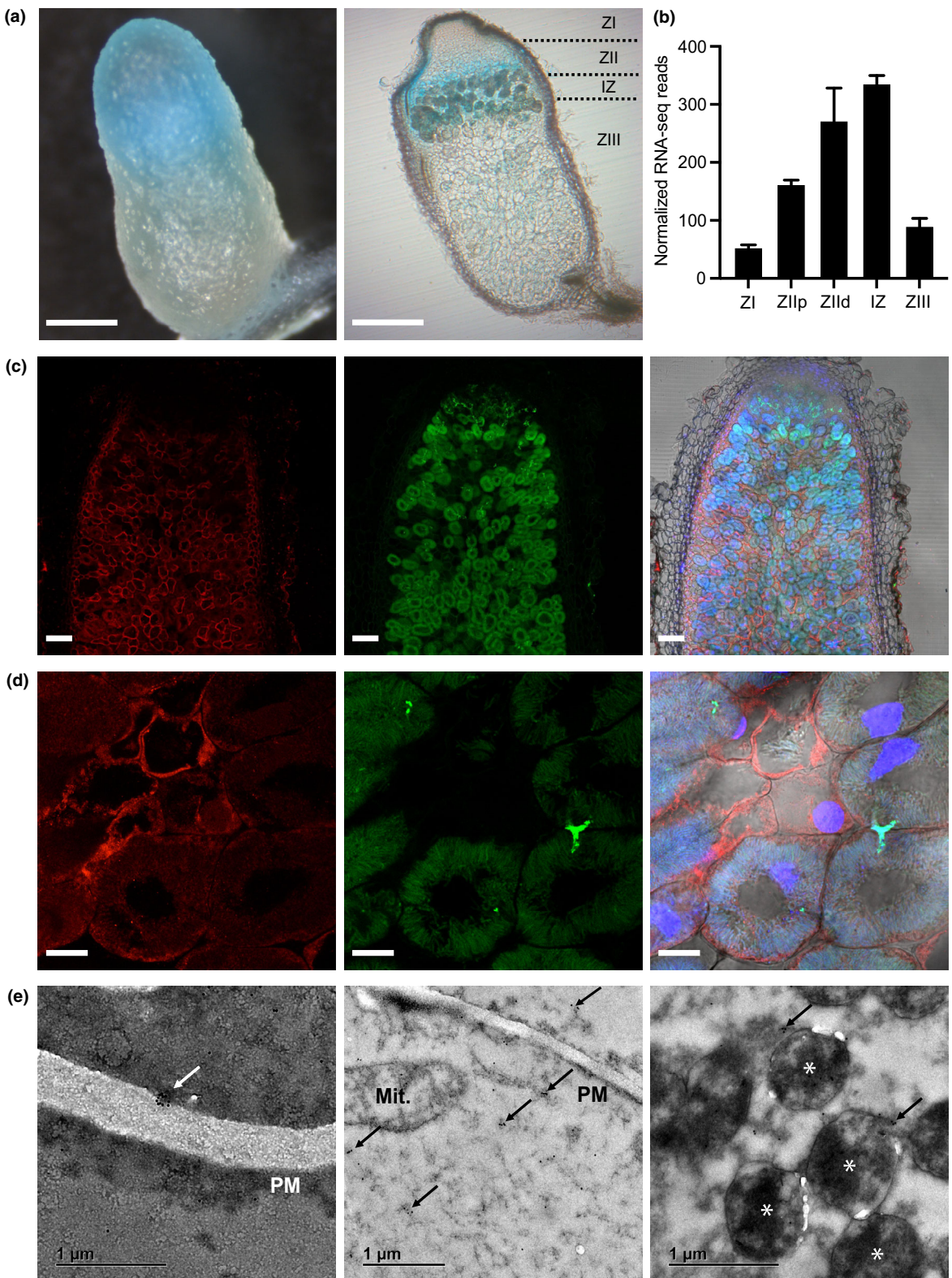


Fig. 3 Localization of MtNCC1 in *Medicago truncatula* nodules. (a) GUS staining of 28 d-postinoculation (dpi) nodules expressing the *gus* gene under the control of the *MtNCC1* promoter region. Left panel shows the whole nodule, and right panel shows a longitudinal section with the different developmental zones indicated. Bars, 400 µm. (b) *MtNCC1* expression in the different nodule zones as indicated in the Symbimics database (<http://ia.nt.toulouse.inra.fr/symbimics/>). ZI, zone I; ZIIp, zone II proximal; ZIId, zone II distal; IZ, interzone; ZIII, zone III. (c) Longitudinal section of 28 dpi *M. truncatula* nodules expressing *MtNCC1* fused to 3 HA domains driven by its own promoter. HA-tagged proteins were detected with using an Alexa594 conjugated antibody (red, left panel). Nodules were colonized by a GFP-expressing *Sinorhizobium meliloti* (green, central panel). DNA was stained with DAPI (blue) and overlaid with the previous two channels and the transillumination signal (right panel). Bars, 100 µm. (d) Closer view of rhizobia-infected cells in zone II. Bars, 10 µm. (e) Immunolocalization of MtNCC1-HA in 28 dpi nodules using gold-conjugated antibodies and electron transmission microscopy. Gold particles are indicated by arrows and asterisks represent bacteroids. PM indicates plasma membrane, and Mit refers to mitochondria. Bars, 1 µm.

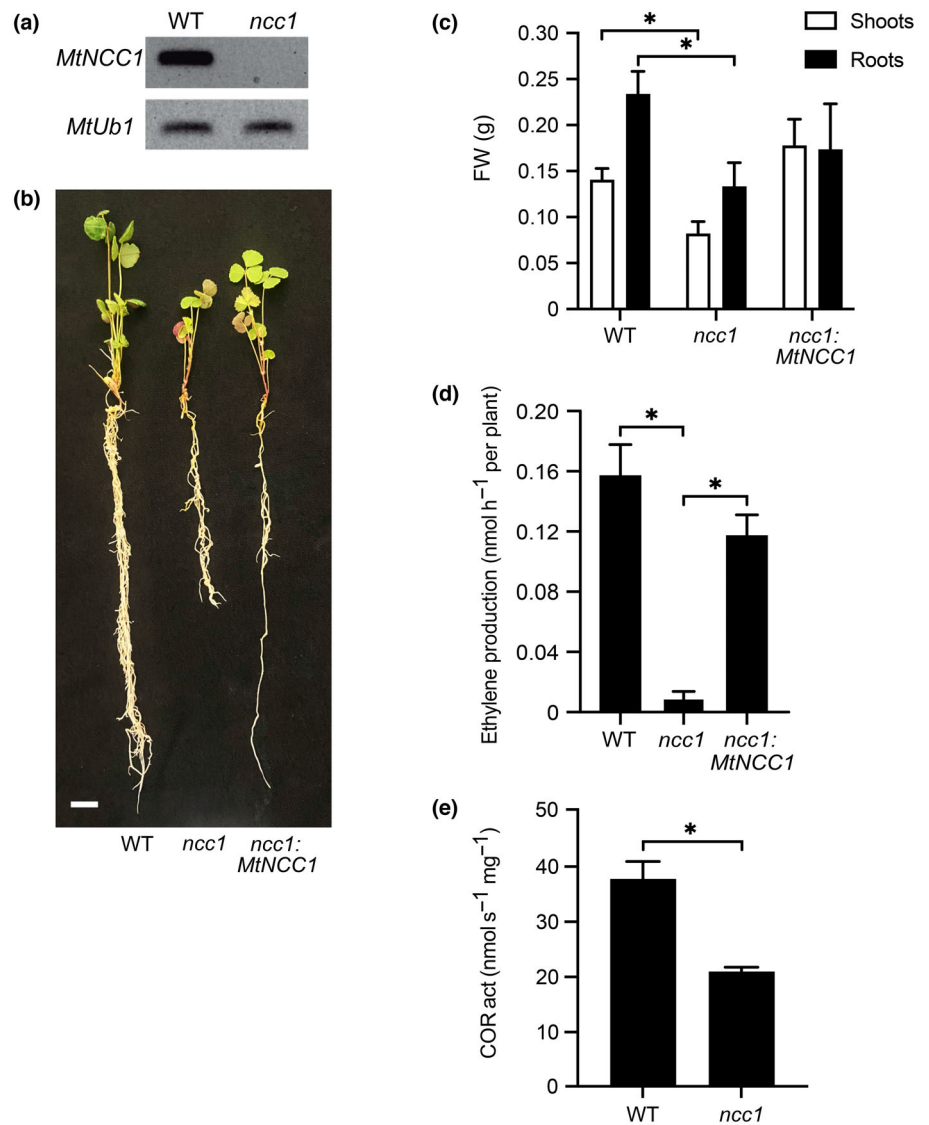


Fig. 4 MtNCC1 is required for nitrogen fixation. (a) Amplification of *MtNCC1* transcript by RT-PCR in 28 d-postinoculation (dpi) nodules of wild-type (WT) and *ncc1* *Medicago truncatula* mutants. *MtUb1* (*Ubiquitin carboxyl-terminal hydrolase 1*) was used as a constitutive gene. (b) Growth of representative plants of WT, *ncc1* mutant and *ncc1* *M. truncatula* mutants transformed with *MtNCC1* regulated by its own promoter. Bar, 1 cm. (c) Fresh weight of shoots and roots of WT, *ncc1* and *ncc1* *M. truncatula* mutants transformed with *MtNCC1* regulated by its own promoter. Data are the mean ± SE ($n = 15$). (d) Acetylene reduction assay in 28 dpi nodules from WT, *ncc1* and *ncc1* *M. truncatula* mutants transformed with *MtNCC1* regulated by its own promoter. Data are the mean ± SE ($n = 7\text{--}13$). (e) Cytochrome oxidase (COX) activity in bacteroids isolated from 28 dpi nodules of WT and *ncc1* *M. truncatula* mutant plants. Data are the mean ± SE of at least three sets of 35–40 pooled plants each. Student's *t*-test was used for statistical analysis (*, $P \leq 0.05$).

Discussion

Symbiotic nitrogen fixation in legume root nodules is a process that requires a large transfer of transition elements from the host plant to the root nodules (O'Hara, 2001; González-Guerrero *et al.*, 2016, 2023). In recent years, many of the transporters mediating this transfer have been identified (Tejada-Jiménez *et al.*, 2015, 2017; Abreu *et al.*, 2017; Senovilla *et al.*, 2018; Castro-Rodríguez *et al.*, 2020; Escudero *et al.*, 2020a,b), as well

as metal-chelating molecules that maintain metal solubility in saps and apoplast (Kryvoruchko *et al.*, 2018; Escudero *et al.*, 2020a). In the case of copper, there is a high degree of specificity in nodules. Host plants, such as *M. truncatula*, express a nodule-specific Cu⁺-uptake transporter, MtCOPT1, to ensure copper uptake by infected cells (Senovilla *et al.*, 2018). Bacteroids also synthesize nodule-specific copper transporters, such as FixI, a P_{1B}-ATPase responsible for providing copper for a nodule-specific high-affinity cytochrome oxidase (Kahn *et al.*, 1989;

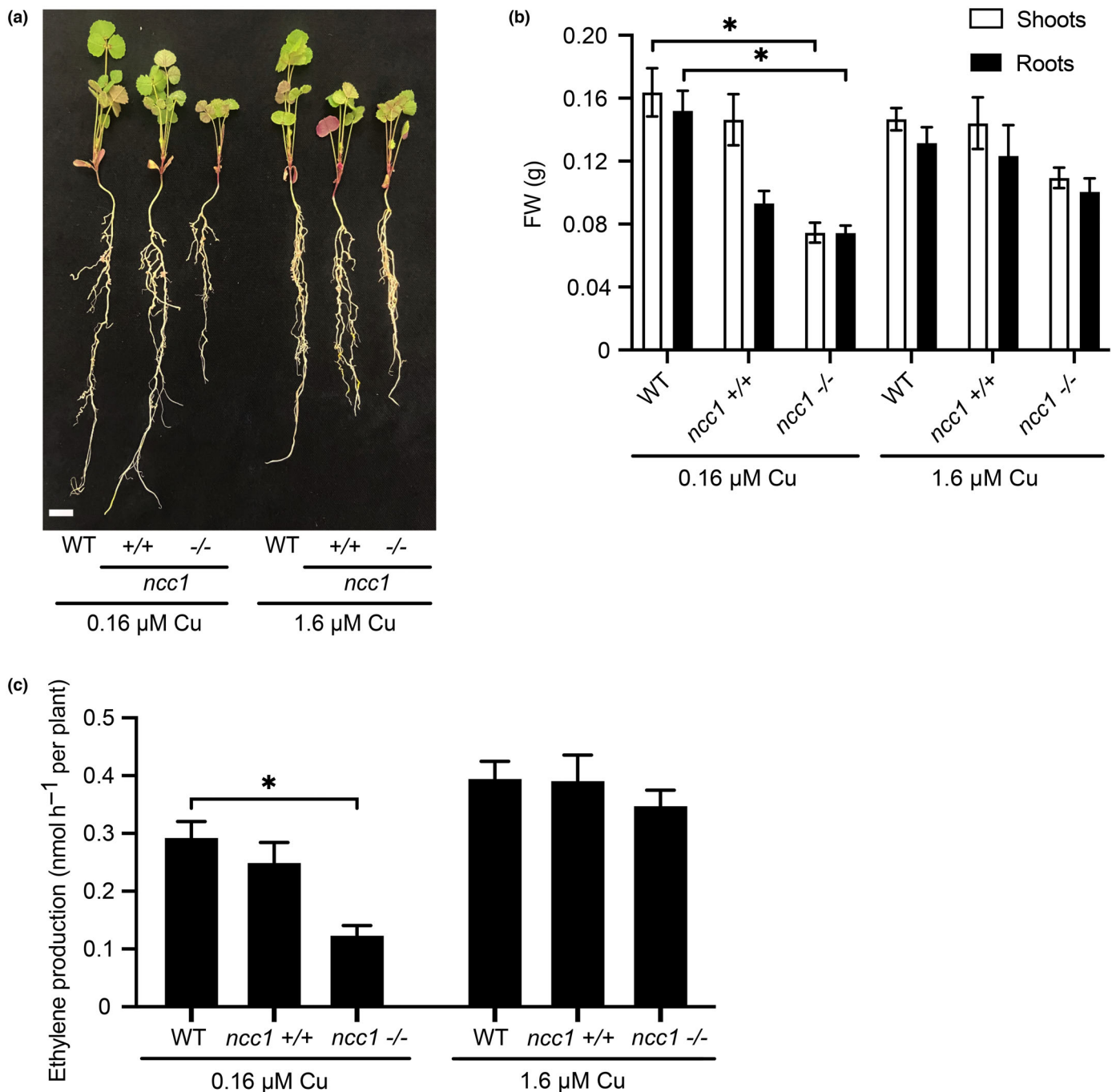


Fig. 5 Copper supplementation complements the *ncc1* phenotype. (a) Growth of representative plants of wild-type (WT) and *ncc1* *Medicago truncatula* mutant watered with standard copper concentrations (0.16 μM) and copper excess (1.6 μM). $^{+/+}$ indicates the WT *ncc1* segregants and $^{-/-}$ the mutant ones. Bar, 1 cm. (b) Fresh weight of shoots and roots of WT and *ncc1* mutant watered with standard copper concentrations (0.16 μM) and copper excess (1.6 μM). Data are the mean \pm SE ($n = 16$ –23). (c) Acetylene reduction assay in 28 d-postinoculation (dpi) nodules from WT and *ncc1* mutant watered with standard copper concentrations (0.16 μM) and copper excess (1.6 μM). Data are the mean \pm SE ($n = 16$ –23). All comparisons were done to WT samples using Student's *t*-test (*, $P \leq 0.05$).

Preisig *et al.*, 1996). However, an additional level of control based on Cu^{+} -chaperones must exist so that copper is specifically delivered from very few copper transporters to multiple different copper enzymes. We have identified MtNCC1 as a representative of this layer of control. The relationship of MtCOPT1 and MtNCC1 roles in nodule copper homeostasis is suggested by the

presence of both proteins in the same nodule zones (mainly from late infection to early fixation zones) and their interaction in BiFC assays. This hints at a functional pairing between the two proteins, the transporter is likely transferring copper to the chaperone. Moreover, MtNCC1 is not the only copper delivery system to symbiosomes. As for *copt1-1*, copper fortification of the

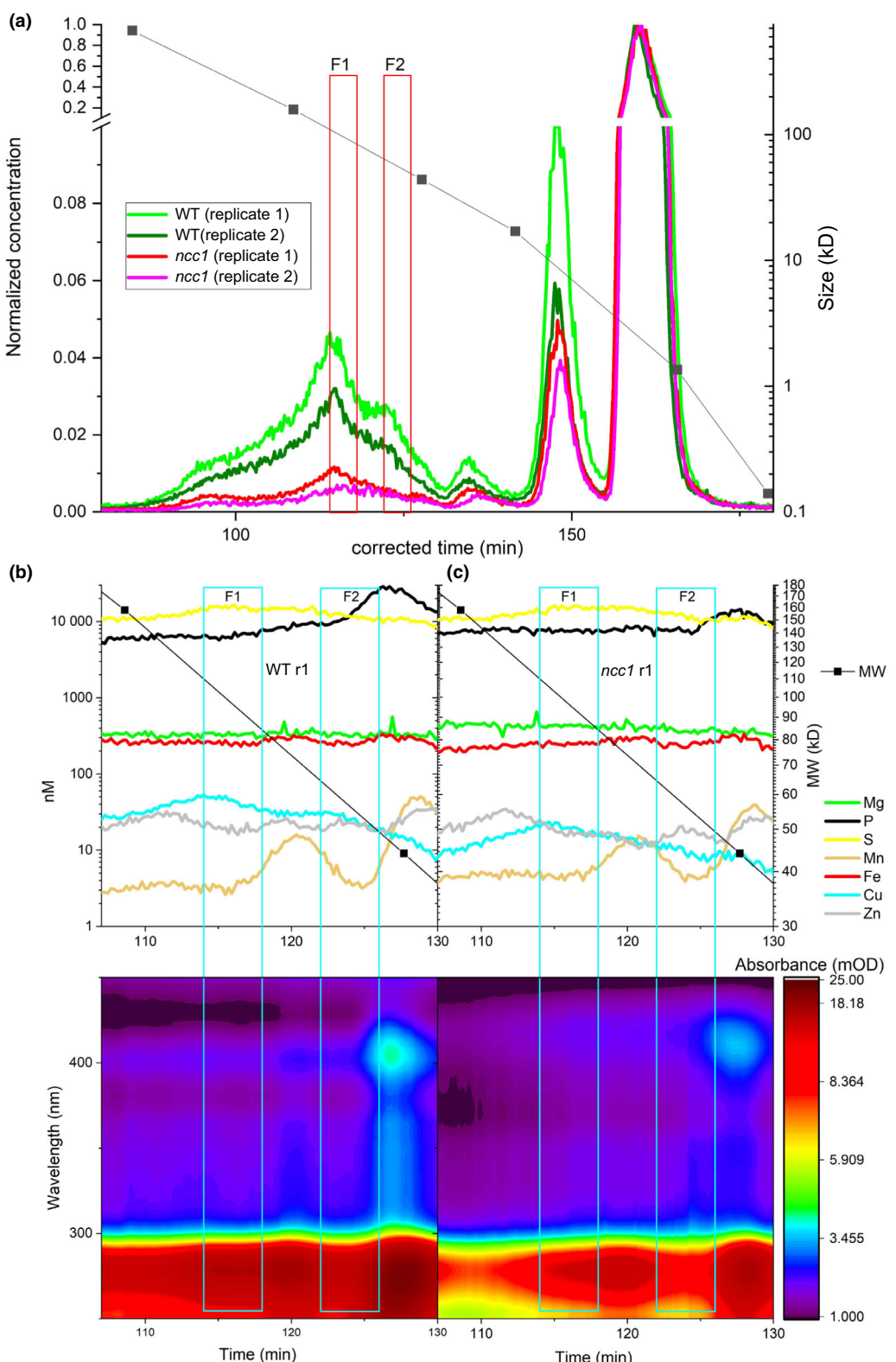


Fig. 6 Mutation of *MtNCC1* alters the nodule copper proteome. (a) Metalloproteomics by HPLC-ICPs-fMS. The normalized chromatograms show copper content in two independent biological replicates of 28 d-postinoculation (dpi) wild-type (WT) and *ncc1* *Medicago truncatula* nodules. Fractions subjected to proteomic analyses are boxed and indicated as F1 and F2. (b, c) Comparison of the most important element chromatograms and UV/VIS absorption DAD in the chromatogram region where the biggest differences between the mutant had been seen in the copper chromatogram: (b) replicate 1 of the WT; (c) replicate 1 of the *ncc1* mutant.

Table 1 Top 10 proteins detected in *Medicago truncatula* wild-type replicates and not in *ncc1* mutant replicates in Fractions 1 or 2 of the metalloproteomic analyses of nodule soluble proteins.

| Uniprot Accession | Organism | Description | Fraction | Connection to copper homeostasis |
|-------------------|----------------------|--|----------|----------------------------------|
| Q4H1G3 | <i>M. truncatula</i> | S-adenosylmethionine synthase | 1 | Zhang et al. (2018) |
| AOA072U7P3 | <i>M. truncatula</i> | Heat-shock cognate 70 kDa protein | 1 | Ahmad et al. (2008) |
| P47923 | <i>M. truncatula</i> | Nucleoside diphosphate kinase 2 | 1 | |
| Q1SL05 | <i>M. truncatula</i> | Putative small GTPase superfamily, P-loop containing nucleoside triphosphate hydrolase | 2 | Gao et al. (2005) |
| G7IEZ9 | <i>M. truncatula</i> | Chalcone-flavonone isomerase family protein 2 | 1 | |
| Q92M81 | <i>S. meliloti</i> | Glyceraldehyde-3-phosphate dehydrogenase | 1 | Chong & Ho (2019) |
| AOA072UDY2 | <i>M. truncatula</i> | Presequence protease | 1 | |
| Q92SW9 | <i>S. meliloti</i> | Recombination protein Rec | 2 | |
| Q92RK3 | <i>S. meliloti</i> | 4-phospho-D-erythronate dehydrogenase | 1 | |
| Q92RH2 | <i>S. meliloti</i> | 3,4-dihydroxy-2-butanone 4-phosphate synthase | 1 | |

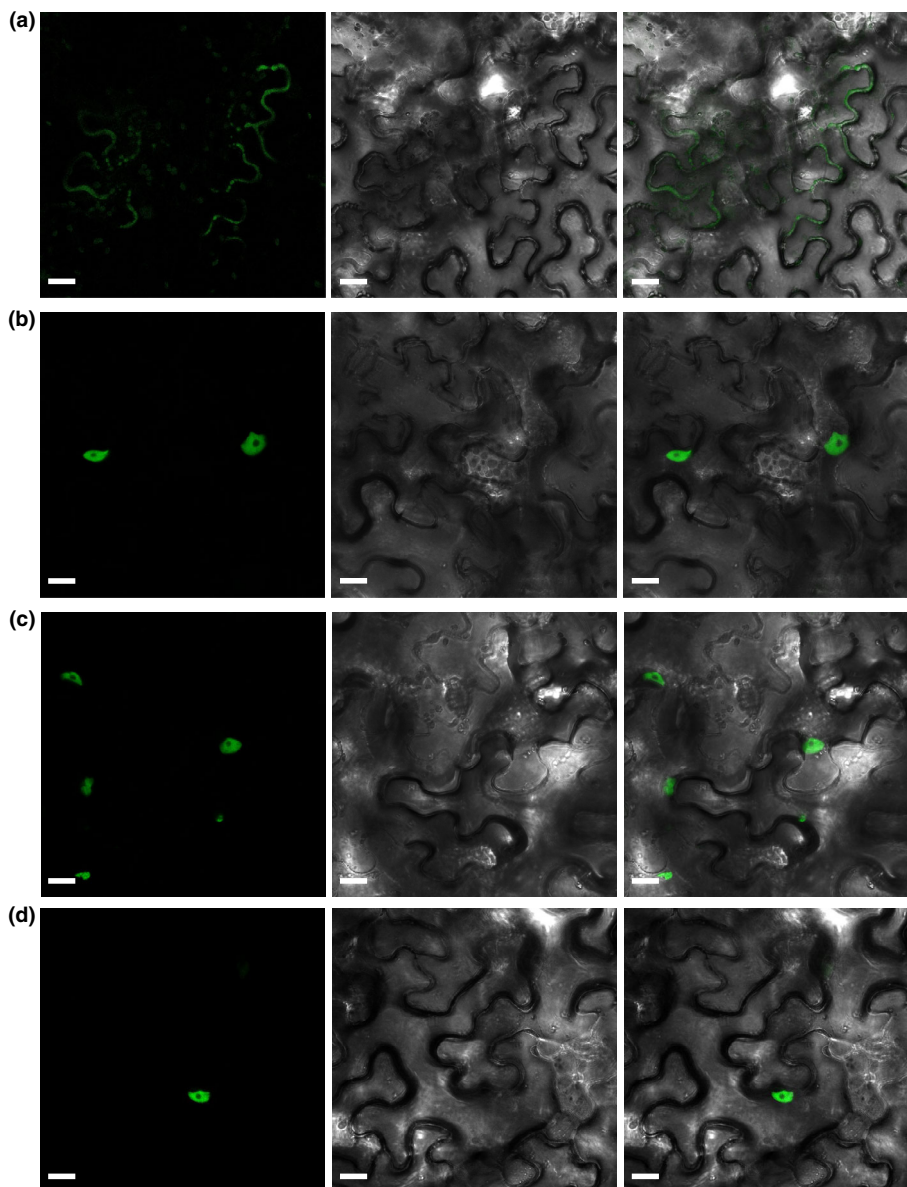


Fig. 7 Bimolecular fluorescent complementation assays of MtNCC1_{1–78} interactions. Transient co-expression of MtNCC1_{1–78} in pNXGW and candidate proteins thioredoxin-dependent peroxiredoxin (a) and SAM synthase (b) in pCXGW, putative universal stress protein A (c) and pathogenesis-related protein (d) in pXCGW, in *N. benthamiana* leaf cells 3 d-postagroinfiltration. Left panel corresponds to the fluorescent signal of MtNCC1_{1–78} and corresponding interactor (green); central panel, transillumination; right panel, overlaid fluorescent image and transillumination images. Bars, 20 µm.

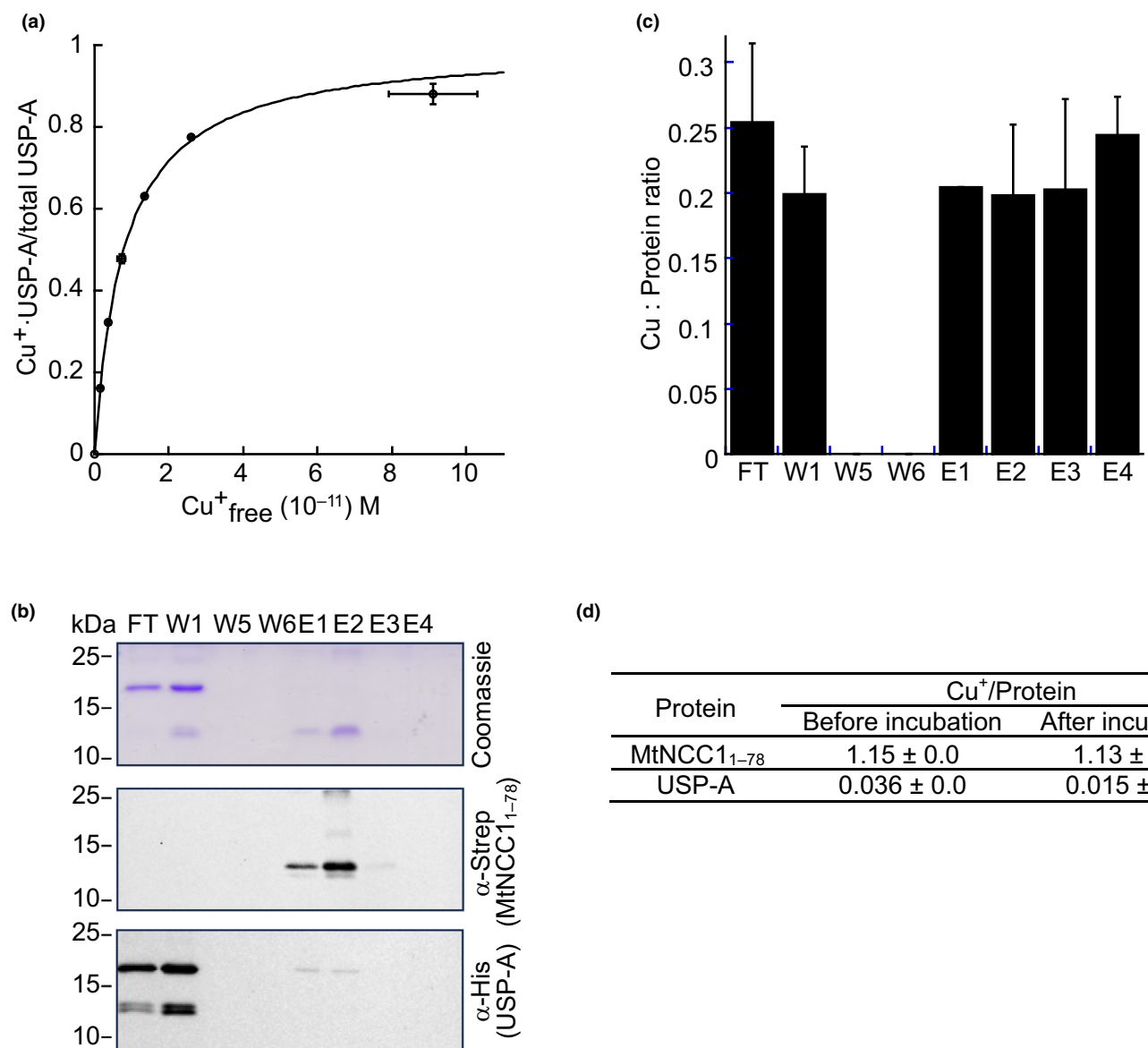


Fig. 8 MtNCC1₁₋₇₈ transfers Cu⁺ to the putative universal stress protein A. (a) Cu⁺ binding to putative USP-A determined in competition assays with BCA. The data were fit using $n = 0.98 \pm 0.02$ Cu⁺ per protein and $K_a = 12.67 \pm 0.05 \text{ pM}^{-1}$. Data are the mean \pm SE (n = 3). (b) Copurification of His₁₀-tagged USP-A with Cu⁺-loaded twin strep-tagged MtNCC1₁₋₇₈ in a Strep-Tactin column. Top panel shows the Coomassie brilliant blue staining the SDS-PAGE gel of the flowthrough (FT), wash (W) and elution (E) fractions. Middle panel corresponds to the immunoblot using an anti-strep antibody. Lower panel is the immunoblot using an anti-His₁₀ antibody. (c) Cu⁺ transfer from MtNCC1₁₋₇₈ to USP-A. The molar copper : protein ratios of the same FT, W and E fractions are shown. Data are the mean \pm SE (n = 3). (d) Lack of Cu⁺ transfer from MtNCC1₁₋₇₈ to USP-A when separated by a dialysis membrane. Data are the mean \pm SE (n = 2).

nutrient solution is sufficient to restore WT growth and nitrogenase activity, suggesting that MtNCC1 is only necessary below a certain copper concentration threshold and that other lower-affinity system(s) can functionally complement MtNCC1. Additionally, MtNCC1 is operating both in infected and noninfected cells, indicating the need for specific copper targeting in both cell types, although to discern the specific function in each cell type, a more detailed study of its interacting partners (localization, cell-specificity and role) would be needed.

The connection between the reduction in nitrogenase activity and mutation of *MtNCC1* is not direct. Nitrogenase does not use

copper as a cofactor, nor is copper known to be directly needed for its synthesis (Burén *et al.*, 2020). In previous studies (Seno-villa *et al.*, 2018), reduction in nitrogenase activity could be explained as the consequence of the reduction in cytochrome oxidase activity that would limit the energy available to bacteroids. However, the partial reduction in cytochrome oxidase activity cannot explain the drastic loss of nitrogenase activity in *ncc1*. The explanation cannot be altered nodule morphology either (WT and *ncc1* nodules do not seem different), nor can it be a collateral effect on iron metabolism in the nodule. The reason must instead lie in the subset of proteins that interact with MtNCC1. Many of

them, when forming complexes with MtNCC1_{1–78} can be detected in the nuclei. Some of them could be involved in epigenetic regulation (SAM synthases; Liu *et al.*, 2020), in the response to plant–microbe interactions (pathogenesis-related proteins; Kaur *et al.*, 2017), or in the coordination between host and bacteroid (nodule-specific cysteine-rich peptides, NCRs) (Maróti *et al.*, 2015), but their specific roles in symbiotic nitrogen fixation still remain to be determined. Our metalloproteomic and pull-down assays have unveiled not only a range of known copper proteins, but also a number of new putative copper proteins that have to be further validated biochemically and placed in the context of symbiotic nitrogen fixation. The initial characterization of the putative USP-A, unveiling it as a new copper protein that can receive this element from MtNCC1, illustrates the path to follow for most of them as it validates the role of MtNCC1 as Cu⁺-chaperone. Other candidate copper proteins might emerge from studying the interaction with the C-terminal domain of MtNCC1. However, all our efforts in that direction were fruitless

because of our failure to recover either full MtNCC1 or C-domain MtNCC1 from the inclusion bodies that formed when they were expressed in *E. coli*.

Interestingly, MtNCC1 is not only located in the cytosol or in the proximity of the membranes; it can also be detected in nuclei, as was the case of CCP in Arabidopsis (Chai *et al.*, 2020). However, no nuclear localization signal could be found in the MtNCC1 sequence. Alternatively, the observed nuclear localization could be the result of interactions with other proteins. The BiFC studies indicate that this is the case, as only some of the interactions tested led to MtNCC1_{1–78} detection in nuclei. The migration of MtNCC1 from cytosol to nucleus will be likely facilitated by importins (Merkle, 2011), some of which have been detected in the pull-down assays. The physiological relevance of this localization is not evident. Theoretically, copper could be delivered to any protein in the cytosol and then the newly metallated proteins could migrate to the nucleus. It could be argued that copper transfer to the nucleus could be conditional to

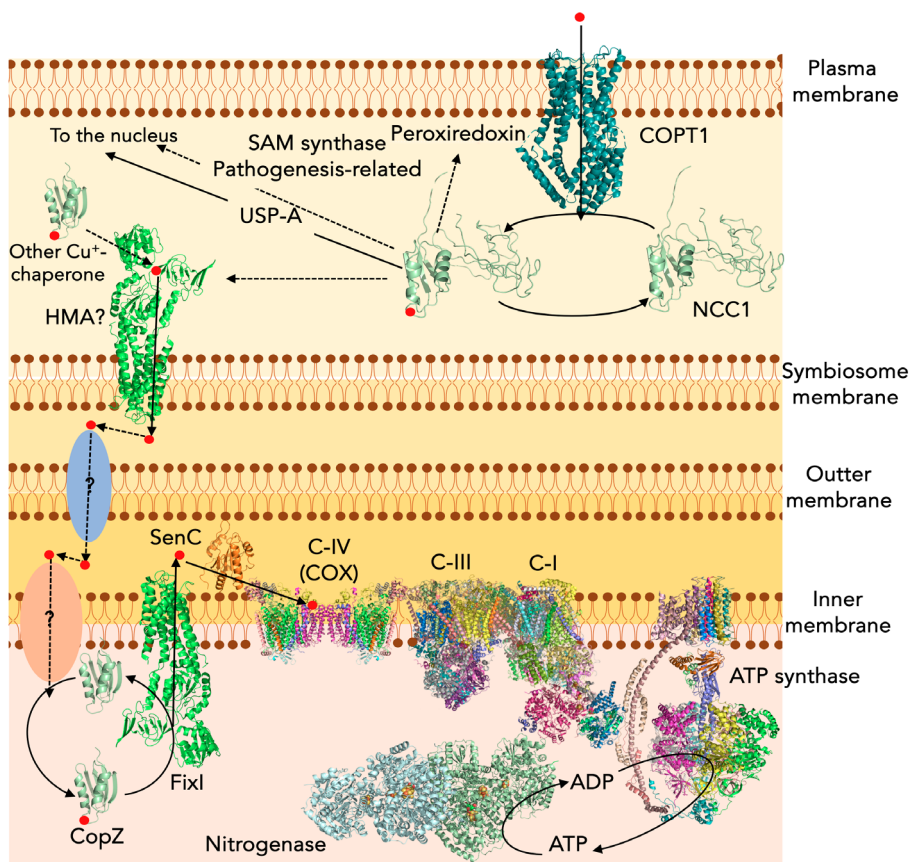


Fig. 9 Model of Cu⁺-transfer processes in symbiotic nitrogen fixation. Copper (red circle) enters the nodule cells through nodule-specific Cu⁺ transporter COPT1, and it is transferred in the cytosolic side to a Cu⁺-chaperone, such as NCC1, by protein–protein interactions. NCC1 provides copper to USP-A protein, and very likely to a SAM synthase, a peroxiredoxin and a pathogenesis-related protein, among others. Interactions with some of these proteins will direct NCC1 to the nucleus. In infected cells, it will also transfer Cu⁺ to the symbiosome copper import transporters, likely Cu⁺-ATPases of the HMA family, although other Cu⁺-chaperones also may carry a similar role. This requires specific docking with the transporter. From there, Cu⁺ reaches the bacteroid cytosol through unknown transporters at the outer and inner membranes. At the cytosol, another Cu⁺-chaperone, CopZ, directs copper to Cu⁺-ATPase Fixl and through SenC is delivered to cytochrome c oxidase (COX). This is essential for the electron transport chain ultimately responsible for providing ATP for nitrogenase functioning. The NCC1 structure model was determined using i-Tasser and AlphaFold. The remaining protein structures were obtained from the Protein Data Bank accessions: 6M98 for COPT1, 5FIL for ATP synthase complex, 1CC7 for Cu⁺-chaperones, 8DH6 for COX complex, 8BPX for complexes I and III, 4HDE for SenC, 3RFU for Cu⁺-ATPases and 8DPN for nitrogenase. Dashed arrows indicate steps in which specific Cu⁺ transfer remains to be confirmed.

specific environmental cues, or that some sort of ternary complex in the nucleus would be needed. These possibilities will have to be specifically tested in the future. However, one role that nuclear MtNCC1 does not seem to play is to deliver Cu⁺ to a putative copper sensor. The existence of a nodule-specific copper sensor can be inferred from the previous work on MtCOPT1. Lack of copper uptake by nitrogen-fixing cells did not result in nodules containing less copper, but the opposite (Senovilla *et al.*, 2018). This was interpreted as a copper-deficiency signal being sent from nodule cells, that led to more copper being delivered. However, since MtCOPT1 was not present, this copper did not reach the cell cytosol and accumulated in the apoplast. This phenotype, however, was not observed in *ncc1* mutants, in which no significant change in copper content was observed when the whole nodule was considered. Only by using, the more discerning metalloproteomic analyses were changes in copper accumulation detected in a subset of the total nodule copper proteome. This illustrates the importance of new approaches of metalloproteomic analysis when assessing metal-dependent phenotypes, particularly when high sensitivity is required; the rest of the copper proteome and other copper-binding molecules (observed in the ICP-MS studies) masked this difference.

Among the candidate MtNCC1_{1–78}, interactor proteins were some proteins that might participate in the unfolded protein response. This, together with the close relationship between Cu⁺-chaperones and HIPP proteins (Tehseen *et al.*, 2010), and HIPP proteins and this response (Guo *et al.*, 2021), could indicate a putative role in stress response. Although such an additional role for MtNCC1 cannot be completely ruled out, it seems unlikely based on the lack of major differences in nodule development, the absence of major signs of stress in nodules, as well as MtNCC1 not presenting the divalent metal cation binding site characteristic of HIPP proteins (Dykema *et al.*, 1999; Zschiesche *et al.*, 2015).

In summary, in this work we have shown the existence of a nodule-specific Cu⁺-chaperone that is required for nitrogen fixation. We propose a model in which MtNCC1 would be accepting Cu⁺ at the plasma membrane from MtCOPT1 (Fig. 9). In rhizobia-colonized cells, Cu⁺ would be transferred to a symbiosome membrane-embedded Cu⁺-efflux transporter, likely a P_{1b}-ATPase (Argüello *et al.*, 2007). Within the symbiosome, Cu⁺ would reach the bacteroid cytosol through yet-to-be-determined transporters at the outer and inner membranes. There, Cu⁺-chaperone CopZ would transfer back the metal to Cu⁺-ATPase FixI (Kahn *et al.*, 1989; Patel *et al.*, 2014) that would be used, in turn, for cytochrome *c* oxidase metallation (Preisig *et al.*, 1996; Andrei *et al.*, 2021). However, in infected and/or noninfected cells MtNCC1 also transfers copper to other proteins such as the putative USP-A identified, and likely a peroxiredoxin, and other proteins involved in plant-microbe interactions, or in SAM metabolism. Some of these interactions result in MtNCC1 being targeted to nuclei. Losing MtNCC1 activity would affect the metallation of these proteins, thus explaining the observed changes in the nodule copper proteome. Future work will be directed to determining the physiological role of these proteins and to verifying that they can accept copper from MtNCC1.

Acknowledgements

This research was funded by grant AGL2018-095996-B-100 from the Ministerio de Ciencia, Innovación/Agencia Estatal de Investigación/10.13039/50110001103 and 'ERDF A way of making Europe' to MG-G. CN-G is supported by Formación de Personal de Investigación fellowship PRE2019-089164 from Ministerio de Ciencia e Innovación/Agencia Estatal de Investigación/10.13039/50110001103 and MR-S by Comunidad de Madrid contract from the Plan de Empleo Juvenil (PEJ-2020-TL-BIO-18547). Metalloproteomics studies were funded by the Ministry of Education, Youth and Sports of the Czech Republic with co-financing from the European Union (grant 'KOROLID', CZ.02.1.01/0.0/0.0/15_003/0000336), the COST association (grant CA19116 'PLANTMETALS') and the Czech Academy of Sciences (RVO: 60077344) to HK. The development of the *M. truncatula* *Tnt1* mutant population was, in part, funded by the National Science Foundation USA grant DBI-0703285. The authors would like to thank Dr Luis Fernández-Pacíos (CBGP, UPM-INIA/CSIC, Spain) for his help with MtNCC1 modelling and Dr Luis Oñate (CBGP, UPM-INIA/CSIC, Spain) for providing the plasmids used for the BiFC assays. We would also like to thank other members of laboratory 279 at Centro de Biotecnología y Genómica de Plantas (UPM-INIA/CSIC) for their support and feedback in preparing this manuscript.

Competing interests

None declared.

Author contributions

CN-G performed most of the experimental work in this manuscript. JL-M contributed to the phenotype and confocal immunolocalization work and carried out the GUS, sequence comparison of *A. thaliana* and *M. truncatula* candidate Cu⁺-chaperones, and the yeast complementation studies. HK and SNHB performed and analysed the metalloproteomic studies. HK did the database mining with focus on bioinorganic chemistry to find which of the proteins found in our study are known to bind copper. MR-S contributed to plasmid generation and plant management. AP-L collaborated in the BiFC studies. JW and KSM produced and characterized the *M. truncatula* *Tnt1* collection. SB optimized MtNCC1_{1–78} purification. JI, VE and MG-G analysed data. VE and MG-G were responsible for overall research supervision and prepared the manuscript with input from all other authors.

ORCID

- Syed Nadeem Hussain Bokhari  <https://orcid.org/0000-0002-7446-8867>
Stefan Burén  <https://orcid.org/0000-0002-8487-2732>
Viviana Escudero  <https://orcid.org/0000-0002-3506-9054>
Manuel González-Guerrero  <https://orcid.org/0000-0001-7334-5286>

- Juan Imperial  <https://orcid.org/0000-0002-5002-6458>
Hendrik Küpper  <https://orcid.org/0000-0003-0712-7023>
Kirankumar S. Mysore  <https://orcid.org/0000-0002-9805-5741>
Cristina Navarro-Gómez  <https://orcid.org/0000-0002-0548-4206>
Alba Paganelli-López  <https://orcid.org/0000-0003-2162-9345>

Data availability

All the data used are included in this manuscript.

References

- Abreu I, Saez A, Castro-Rodríguez R, Escudero V, Rodríguez-Haas B, Senovilla M, Larue C, Grolimund D, Tejada-Jiménez M, Imperial J *et al.* 2017. *Medicago truncatula* Zinc-Iron Permease6 provides zinc to rhizobia-infected nodule cells. *Plant, Cell & Environment* 40: 2706–2719.
- Ahmad MF, Singh D, Taiyab A, Ramakrishna T, Raman B, Rao CM. 2008. Selective Cu²⁺ binding, redox silencing, and cytoprotective effects of the small heat shock proteins αA- and αB-crystallin. *Journal of Molecular Biology* 382: 812–824.
- Andrei A, Di Renzo MA, Öztürk Y, Meisner A, Daum N, Frank F, Rauch J, Daldal F, Andrade SLA, Koch HG. 2021. The CopA2-type ATPase CcoI serves as central hub for *cbb₃*-type cytochrome oxidase biogenesis. *Frontiers in Microbiology* 12: 712465.
- Andresen E, Kappel S, Stärk HJ, Rieger U, Borovec J, Mattusch J, Heinz A, Schmelzer CEH, Matoušková Š, Dickinson B *et al.* 2016. Cadmium toxicity investigated at the physiological and biophysical levels under environmentally relevant conditions using the aquatic model plant *Ceratophyllum demersum* L. *New Phytologist* 210: 1244–1258.
- Andresen E, Peiter E, Küpper H. 2018. Trace metal metabolism in plants. *Journal of Experimental Botany* 69: 909–954.
- Argiello JM, Eren E, González-Guerrero M. 2007. The structure and function of heavy metal transport P_{1B}-ATPases. *Biometals* 20: 233–2348.
- Attallah C, Welchen E, Martin AP, Spinelli SV, Bonnard G, Palatnik JF, Gonzalez DH. 2011. Plants contain two SCO proteins that are differentially involved in cytochrome *c* oxidase function and copper and redox homeostasis. *Journal of Experimental Botany* 62: 4281–4294.
- Blaby-Haas CE, Padilla-Benavides T, Stübe R, Argiello JM, Merchant SS. 2014. Evolution of a plant-specific copper chaperone family for chloroplast copper homeostasis. *Proceedings of the National Academy of Sciences, USA* 111: E5480–E5487.
- Boisson-Dernier A, Chabaud M, Garcia F, Bécard G, Rosenberg C, Barker DG. 2001. *Agrobacterium rhizogenes*-transformed roots of *Medicago truncatula* for the study of nitrogen-fixing and endomycorrhizal symbiotic associations. *Molecular Plant-Microbe Interactions* 14: 695–700.
- Bradford MM. 1976. A rapid and sensitive method for the quantitation of microgram quantities of protein utilizing the principle of protein-dye binding. *Analytical Biochemistry* 7: 248–254.
- Brenner AJ, Harris ED. 1995. A quantitative test for copper using bicinchoninic acid. *Analytical Biochemistry* 226: 80–84.
- Brito B, Palacios JM, Hidalgo E, Imperial J, Ruiz-Argüeso T. 1994. Nickel availability to pea (*Pisum sativum* L.) plants limits hydrogenase activity of *Rhizobium leguminosarum* bv. *viciae* bacteroids by affecting the processing of the hydrogenase structural subunits. *Journal of Bacteriology* 176: 5297–5303.
- Burén S, Jiménez-Vicente E, Echavarri-Erasun C, Rubio LM. 2020. Biosynthesis of nitrogenase cofactors. *Chemical Reviews* 120: 4921–4968.
- Burkhead JL, Gogolin Reynolds KA, Abdel-Ghany SE, Cohu CM, Pilon M. 2009. Copper homeostasis. *New Phytologist* 182: 799–816.
- Castro-Rodríguez R, Abreu I, Reguera M, Novoa-Aponte L, Mijovilovich A, Escudero V, Jiménez-Pastor FJ, Abadía J, Wen J, Mysore KS *et al.* 2020. The *Medicago truncatula* Yellow Stripe1-Like3 gene is involved in vascular delivery of transition metals to root nodules. *Journal of Experimental Botany* 71: 7257–7269.
- Chai LX, Dong K, Liu SY, Zhang Z, Zhang XP, Tong X, Zhu FF, Zou JZ, Wang XB. 2020. A putative nuclear copper chaperone promotes plant immunity in *Arabidopsis*. *Journal of Experimental Botany* 71: 6684–6696.
- Changella A. 2003. Molecular basis of metal-ion selectivity and zeptomolar sensitivity by CueR. *Science* 301: 1383–1397.
- Cheng HP, Walker GC. 1998. Succinoglycan is required for initiation and elongation of infection threads during nodulation of alfalfa by *Rhizobium meliloti*. *Journal of Bacteriology* 180: 5183–5191.
- Chong IKW, Ho WS. 2019. Glyceraldehyde-3-phosphate dehydrogenase from Chironomidae showed differential activity towards metals. *Protein & Peptide Letters* 20: 970–976.
- Chu CC, Lee WC, Guo WY, Pan SM, Chen LJ, Li H, Jinn TL. 2005. A copper chaperone for superoxide dismutase that confers three types of copper/zinc Superoxide dismutase activity in *Arabidopsis*. *Plant Physiology* 139: 425–436.
- Deblaere R, Bytebier B, de Greve H, Deboeck F, Schell J, van Montagu M, Leemans J. 1985. Efficient octopine Ti plasmid-derived vectors for *Agrobacterium*-mediated gene transfer to plants. *Nucleic Acids Research* 13: 4777.
- Dimmer KS, Fritz S, Fuchs F, Messerschmitt M, Weinbach N, Neupert W, Westermann B. 2002. Genetic basis of mitochondrial function and morphology in *Saccharomyces cerevisiae*. *Molecular Biology of the Cell* 13: 847–853.
- Downie JA. 2014. Legume nodulation. *Current Biology* 24: R184–R190.
- Dykema PE, Sipes PR, Marie A, Biermann BJ, Crowell DN, Randall SK. 1999. A new class of proteins capable of binding transition metals. *Plant Molecular Biology* 41: 139–150.
- Eren E, González-Guerrero M, Kaufman B, Argüello JM. 2007. Novel Zn²⁺ coordination by the regulatory N-terminus metal binding domain of *Arabidopsis thaliana* Zn²⁺-ATPase HMA2. *Biochemistry* 46: 7754–7764.
- Escudero V, Abreu I, del Sastre E, Tejada-Jiménez M, Larue C, Novoa-Aponte L, Castillo-González J, Wen J, Mysore KS *et al.* 2020a. Nicotianamine Synthase 2 is required for symbiotic nitrogen fixation in *Medicago truncatula* nodules. *Frontiers in Plant Science* 10: 1780.
- Escudero V, Abreu I, Tejada-Jiménez M, Rosa-Núñez E, Quintana J, Prieto RI, Larue C, Wen J, Villanova J, Mysore KS *et al.* 2020b. *Medicago truncatula* Ferroportin2 mediates iron import into nodule symbiosomes. *New Phytologist* 228: 194–209.
- Flis P, Ouerdane L, Grillet L, Curie C, Mari S, Lobinski R. 2016. Inventory of metal complexes circulating in plant fluids: a reliable method based on HPLC coupled with dual elemental and high-resolution molecular mass spectrometric detection. *New Phytologist* 211: 1129–1141.
- Gao X, Ziyun D, Patel TB. 2005. Copper and zinc inhibit Galphas function: a nucleotide-free state of Galphas induced by Cu²⁺ and Zn²⁺. *Journal of Biological Chemistry* 280: 2579–2586.
- Goldstein S, Meyerstein D, Czapski G. 1993. The Fenton reagents. *Free Radical Biology and Medicine* 15: 435–445.
- González-Guerrero M, Argüello JM. 2008. Mechanism of Cu⁺-transporting ATPases: soluble Cu⁺ chaperones directly transfer Cu⁺ to transmembrane transport sites. *Proceedings of the National Academy of Sciences, USA* 105: 5992–5997.
- González-Guerrero M, Escudero V, Sáez Á, Tejada-Jiménez M. 2016. Transition metal transport in plants and associated endosymbionts *Arbuscular mycorrhizal* fungi and rhizobia. *Frontiers in Plant Science* 7: 1088.
- González-Guerrero M, Navarro-Gómez C, Rosa-Núñez E, Echávarri-Erasun C, Imperial J, Escudero V. 2023. Forging a symbiosis: transition metal delivery in symbiotic nitrogen fixation. *New Phytologist* 239: 2113–2125.
- González-Guerrero M, Raimunda D, Cheng X, Argüello JM. 2010. Distinct functional roles of homologous Cu⁺ efflux ATPases in *Pseudomonas aeruginosa*. *Molecular Microbiology* 78: 1246–1258.
- Guo T, Weber H, Niermann MCE, Theisl L, Leonte G, Novál O, Werner T. 2021. *Arabidopsis* HIPP proteins regulate endoplasmic reticulum-associated degradation of CKX proteins and cytokinin responses. *Molecular Plant* 14: 1918–1934.
- Hamilton GA, Libby RD, Hartzell CR. 1973. The valence of copper and the role of superoxide in the D-galactose oxidase catalyzed reaction. *Biochemical and Biophysical Research Communications* 55: 333–340.

- Hardy RWF, Holsten RD, Jackson EK, Burns RC. 1968. The acetylene-ethylene assay for N₂ fixation: laboratory and field evaluation. *Plant Physiology* 43: 1185–1207.
- Johnston AW, Yeoman KH, Wexler M. 2001. Metals and the rhizobial-legume symbiosis – uptake, utilization and signalling. *Advances in Microbial Physiology* 45: 113–156.
- Kahn D, David M, Domergue O, Daveran ML, Ghai J, Hirsch PR, Battu J. 1989. *Rhizobium meliloti* fixGHI sequence predicts involvement of a specific cation pump in symbiotic nitrogen fixation. *Journal of Bacteriology* 171: 929–939.
- Kaur A, Pati PK, Pati AM, Nagpal AK. 2017. *In-silico* analysis of *cis*-acting regulatory elements of pathogenesis-related proteins of *Arabidopsis thaliana* and *Oryza sativa*. *PLoS ONE* 12: e0184523.
- Kim JG, Li X, Roden JA, Taylor KW, Aakre CD, Su B, Lalonde S, Kirik A, Chen Y, Baranage G et al. 2009. *Xanthomonas* T3S effector XopN suppresses PAMP-triggered immunity and interacts with a tomato atypical receptor-like kinase and TFT1. *Plant Cell* 21: 1305–1323.
- Kryvoruchko IS, Routray P, Sinharoy S, Torres-Jerez I, Tejada-Jiménez M, Finney LA, Nakashima J, Pislaru CI, Benedito VA, González-Guerrero M et al. 2018. An iron-activated citrate transporter, MtMATE67, is required for symbiotic nitrogen fixation. *Plant Physiology* 176: 2315–2329.
- Küpper H, Andresen E. 2016. Mechanisms of metal toxicity in plants. *Metalomics* 8: 269–285.
- Küpper H, Bokhari SNH, Jaime-Pérez N, Lyubenova L, Ashraf N, Andresen E. 2019. Ultratrace metal speciation analysis by coupling of sector-field ICP-MS to high-resolution size exclusion and reversed-phase liquid chromatography. *Analytical Chemistry* 91: 10961–10969.
- Küpper H, Küpper F, Spiller M. 1996. Environmental relevance of heavy metal substituted chlorophylls using the example of submersed water plants. *Journal of Experimental Botany* 47: 259–266.
- Küpper H, Šetlík I, Spiller M, Küpper FC, Prášil O. 2002. Heavy metal-induced inhibition of photosynthesis: targets of *in vivo* heavy metal chlorophyll formation. *Journal of Phycology* 38: 429–441.
- Li L, Kaplan J. 2001. The yeast gene MSC2, a member of the cation diffusion facilitator family, affects the cellular distribution of zinc. *Journal of Biological Chemistry* 276: 5036–5043.
- Lin SJ, Pufahl RA, Dancis A, O'Halloran TV, Culotta VC. 1997. A role for the *Saccharomyces cerevisiae* ATX1 gene in copper trafficking and iron transport. *Journal of Biological Chemistry* 272: 9215–9220.
- Liu M, Saha N, Gajan A, Saadat N, Gupta SV, Pile LA. 2020. A complex interplay between SAM synthetase and the epigenetic regulator SIN3 controls metabolism and transcription. *Journal of Biological Chemistry* 295: 375–389.
- Macomber L, Imlay JA. 2009. The iron-sulfur clusters of dehydratases are primary intracellular targets of copper toxicity. *Proceedings of the National Academy of Sciences, USA* 106: 8344–8349.
- Maróti G, Downie JA, Kondorosi E. 2015. Plant cysteine-rich peptides that inhibit pathogen growth and control rhizobial differentiation in legume nodules. *Current Opinion on Plant Biology* 26: 57–63.
- Marschner P. 2011. *Mineral nutrition of higher plants*, 3rd edn. Amsterdam, the Netherlands: Academic Press.
- Merkle T. 2011. Nucleo-cytoplasmic transport of proteins and RNA in plants. *Plant Cell Reports* 30: 153–176.
- Mira H, Martínez-García F, Peñarrubia L. 2001. Evidence for the plant-specific intercellular transport of the *Arabidopsis* copper chaperone CCH. *The Plant Journal* 25: 521–528.
- Nakagawa T, Kurose T, Hino T, Tanaka K, Kawamukai M, Niwa Y, Toyooka K, Matsuo K, Jinbo T, Kimura T. 2007. Development of series of gateway binary vectors, pGWBs, for realizing efficient construction of fusion genes for plant transformation. *Journal of Bioscience and Bioengineering* 104: 34–41.
- Narindrorasarak S, Yao P, Sarkar B. 2003. Protein disulfide isomerase, a multifunctional protein chaperone, shows copper-binding activity. *Biochemical and Biophysical Research Communications* 311: 405–414.
- O'Hara GW. 2001. Nutritional constraints on root nodule bacteria affecting symbiotic nitrogen fixation: a review. *Australian Journal of Experimental Agriculture* 41: 417–433.
- Palumaa P, Kangur L, Voronova A, Sillard R. 2004. Metal-binding mechanism of Cox17, a copper chaperone for cytochrome c oxidase. *Biochemical Journal* 382: 307–314.
- Patel SJ, Padilla-Benavides T, Collins JM, Argüello JM. 2014. Functional diversity of five homologous Cu⁺-ATPases present in *Sinorhizobium meliloti*. *Microbiology* 160: 1237–1251.
- Preisig O, Zufferey R, Thony-Meyer L, Appleby CA, Hennecke H. 1996. A high-affinity cbb3-type cytochrome oxidase terminates the symbiosis-specific respiratory chain of *Bradyrhizobium japonicum*. *Journal of Bacteriology* 178: 1532–1538.
- Rae TD, Schmidt PJ, Pufahl RA, Culotta VC, O'Halloran TV. 1999. Undetectable intracellular free copper: the requirement of a copper chaperone for superoxide dismutase. *Science* 284: 805–808.
- Robinson NJ, Winge DR. 2010. Copper metallochaperones. *Annual Review in Biochemistry* 79: 537–562.
- Schiestl RH, Gietz RD. 1989. High efficiency transformation of intact yeast cells using single stranded nucleic acids as a carrier. *Current Genetics* 16: 339–346.
- Schlutz LW, Chivers PT, Raines RT. 1999. The CXXC motif: crystal structure of an active-site variant of *Escherichia coli* thioredoxin. *Acta Crystallographica D55*: 1533–1538.
- Senovilla M, Castro-Rodríguez R, Abreu I, Escudero V, Kryvoruchko I, Udvardi MK, Imperial J, González-Guerrero M. 2018. *Medicago truncatula* copper transporter 1 (MtCOPT1) delivers copper for symbiotic nitrogen fixation. *New Phytologist* 218: 696–709.
- Sherman F, Fink GR, Hicks JB. 1983. *Methods in yeast genetics*. Cold Spring Harbour Lab.
- Shin LJ, Lo JC, Yeh KC. 2012. Copper chaperone antioxidant protein1 is essential for copper homeostasis. *Plant Physiology* 159: 1099–1110.
- Soma S, Latimer AJ, Chun H, Vicary AC, Timbalia SA, Boulet A, Rahn JJ, Chan SSL, Leary SC, Kim BEK et al. 2018. Elesclomol restores mitochondrial function in genetic models of copper deficiency. *Proceedings of the National Academy of Sciences, USA* 115: 8161–8166.
- Tehseen M, Cairns N, Sherson S, Cobbett CS. 2010. Metallochaperone-like genes in *Arabidopsis thaliana*. *Metalomics* 2: 556–564.
- Tejada-Jiménez M, Castro-Rodríguez R, Kryvoruchko I, Lucas MM, Udvardi M, Imperial J, González-Guerrero M. 2015. *Medicago truncatula* natural resistance-associated macrophage protein 1 is required for iron uptake by rhizobia-infected nodule cells. *Plant Physiology* 168: 258–272.
- Tejada-Jiménez M, Gil-Diez P, Leon-Medaivilla J, Wen J, Mysore KS, Imperial J, González-Guerrero M. 2017. *Medicago truncatula* Molybdate Transporter type 1 (MOT1.3) is a plasma membrane molybdenum transporter required for nitrogenase activity in root nodules under molybdenum deficiency. *New Phytologist* 216: 1223–1235.
- Udvardi M, Poole PS. 2013. Transport and metabolism in legume-rhizobia symbioses. *Annual Review in Plant Biology* 64: 781–805.
- Vasse J, de Billy F, Camut S, Truchet G. 1990. Correlation between ultrastructural differentiation of bacteroids and nitrogen fixation in alfalfa nodules. *Journal of Bacteriology* 172: 4295–4306.
- Vernoud V, Journet EP, Barker DG. 2007. MtENOD20, a Nod factor-inducible molecular marker for root cortical cell activation. *Molecular Plant–Microbe Interactions* 12: 604–614.
- Wong PC, Waggoner D, Subramanian JR, Tessarollo L, Bartnikas TB, Culotta VC, Price DL, Rothstein J, Gitlin JD. 2000. Copper chaperone for superoxide dismutase is essential to activate mammalian Cu/Zn superoxide dismutase. *Proceedings of the National Academy of Sciences, USA* 97: 2886–2891.
- Wood WB. 1996. Host specificity of DNA produced by *Escherichia coli*: bacterial mutations affecting the restriction and modification of DNA. *Journal of Molecular Biology* 16: 118–133.
- Xiao TT, Schilderink S, Moling S, Deinum EE, Kondorosi E, Franssen H, Kulikova O, Niebel A, Bisseling T. 2014. Fate map of *Medicago truncatula* root nodules. *Development* 141: 3517–3528.
- Yatsunyk LA, Rosenzweig AC. 2007. Cu(I) binding and transfer by the N terminus of the Wilson disease protein. *Journal of Biological Chemistry* 282: 8622–8631.
- Zhang B, Liu H, Ding X, Qiu J, Zhang M, Chu Z. 2018. *Arabidopsis thaliana* ACS8 plays a crucial role in the early biosynthesis of ethylene elicited by Cu²⁺ ions. *Journal of Cell Science* 131: jcs202424.

Zschiesche W, Barth O, Daniel K, Böhme S, Rausche J, Humbeck K. 2015. The zinc-binding nuclear protein HIPP3 acts as an upstream regulator of the salicylate-dependent plant immunity pathway and of flowering time in *Arabidopsis thaliana*. *New Phytologist* 207: 1084–1096.

Supporting Information

Additional Supporting Information may be found online in the Supporting Information section at the end of the article.

Fig. S1 Putative Cu⁺-chaperones in *Arabidopsis thaliana* and *Medicago truncatula*.

Fig. S2 *MtNCC1* expression in nodules and roots.

Fig. S3 Purification of MtNCC1_{1–78}.

Fig. S4 Cu⁺-binding to MtNCC_{1–78}.

Fig. S5 Negative control for BiFC.

Fig. S6 Control for immunolocalization.

Fig. S7 Immunolocalization of MtNCC1_{1–78}-HA.

Fig. S8 MtNCC1 is not necessary during nonsymbiotic conditions.

Fig. S9 Development of *ncc1* mutant nodules compared with wild-type ones.

Fig. S10 Nitrogenase activity of wild-type and *ncc1* nodules referred to nodule biomass.

Fig. S11 Mutation of *MtNCC1* does not alter the nodule metal-lome.

Fig. S12 Complete HPLC-ICPs-fMS chromatograms.

Fig. S13 Putative Cu⁺-binding site in putative universal stress protein A (*Medtr1g088640*).

Fig. S14 Negative control for BiFC.

Fig. S15 Purification of the putative universal stress protein A.

Methods S1 Supplementary materials and methods.

Table S1 Primers used in this study.

Table S2 Expression profile of candidate Cu⁺-chaperones and HIPP proteins in nodules.

Table S3 Proteins identified in Fraction 1.

Table S4 Proteins identified in Fraction 2.

Table S5 Proteins identified in MtNCC1_{1–78} pull-down assay.

Table S6 Proteins found both in pull-down assay and in Fractions 1 or 2 of the metalloproteomic analyses.

Please note: Wiley is not responsible for the content or functionality of any Supporting Information supplied by the authors. Any queries (other than missing material) should be directed to the *New Phytologist* Central Office.